Thermoelectric silicides: A review

2017 Jpn. J. Appl. Phys. 56 05DA04

(http://iopscience.iop.org/1347-4065/56/5S1/05DA04)

Japanese Journal of Applied Physics **56**, 05DA04 (2017)
https://doi.org/10.7567/JJAP.56.05DA04

PROGRESS REVIEW

Thermoelectric silicides: A review

Amin Nozariasbmarz[1,2], Aditi Agarwal[1], Zachary A. Coutant[1], Michael J. Hall[2], Jie Liu[1], Runze Liu[1], Abhishek Malhotra[1], Payam Norouzzadeh[1], Mehmet C. Öztürk[1], Viswanath P. Ramesh[1], Yasaman Sargolzaeiaval[1], Francisco Suarez[1], and Daryoosh Vashaee[1,2*]

[1]*Electrical and Computer Engineering Department, Monteith Research Center, North Carolina State University, Raleigh, NC 27606, U.S.A.*
[2]*Material Science and Engineering Department, Monteith Research Center, North Carolina State University, Raleigh, NC 27606, U.S.A.*

*E-mail: dvashae@ncsu.edu
†The names after the first author are listed alphabetically. All authors contributed equally in this work.

Received October 2, 2016; accepted November 27, 2016; published online March 3, 2017

Traditional research on thermoelectric materials focused on improving the figure-of-merit zT to enhance the energy conversion efficiency. With further growth and commercialization of thermoelectric technology beyond niche applications, other factors such as materials availability, toxicity, cost, recyclability, thermal stability, chemical and mechanical properties, and ease of fabrication become important for making viable technologies. Several silicide alloys were identified that have the potential to fulfill these requirements. These materials are of interest due to their abundancy in earth's crust (e.g., silicon), non-toxicity, and good physical and chemical properties. In this paper, an overview of the silicide thermoelectrics from traditional alloys to advanced material structures is presented. In addition, some of the most effective approaches as well as fundamental physical concepts for designing and developing efficient thermoelectric materials are presented and future perspectives are discussed.

1. Introduction

Thermoelectric generators with the ability to produce useful electric power from low-grade or waste heat can play a significant role in reducing carbon emissions and mitigating global warming. Over the past two decades, thermoelectric technology has made significant scientific progress and many good thermoelectric materials have been developed for their use in clean and sustainable energy sources. A good thermoelectric material has large electrical conductivity, σ, high Seebeck coefficient, S, and low thermal conductivity, κ, resulting in a large dimensionless-figure-of-merit, zT, where $zT = S^2\sigma T/\kappa$, in which T is the absolute temperature. The efforts to find or develop good thermoelectric materials mainly followed two directions. The first approach is finding new bulk materials and their further engineering to increase their zT.[1,2] Some examples representative of this direction are the filled skutterudites,[3] such as $Sr_{0.16}Yb_{0.03}Co_4Sb_{12}$,[4] clathrates, such as $Ba_8Ga_{16}Ge_{30}$,[5] Zintl phases, such as $Yb_{14}Mn_{1-x}Al_xSb_{11}$,[6] metal silicides, such as $Mg_2Si_{1-x}Sn_x$, and other materials such as $(GeTe)_{75}(AgSbTe_2)_{25}$ (TAGS-75),[7] $AgPb_{18}SbTe_{20}$ (LAST),[8] PbTe(Tl),[9] and SnSe.[10] Another direction is the use of nanostructures (e.g., superlattices) that improve the power factor ($S^2\sigma$) through quantum size effects,[11–13] or interface energy filtering,[14–16] while their thermal conductivity is reduced through scattering of phonons at interfaces.[12,17] Some examples of these groups include ErAs rare earth nanocomposites and ScN/ZrWN multilayers for thermoelectric energy conversion.[18–21] The improved zT in these structures comes mainly from the reduction in phonon thermal conductivity and to a lesser extent, from enhancing the power factor. Nanostructured bulk Bi_2Te_3[22–24] and PbTe[25] based materials have also shown to have high zT, resulting from their incorporation of nano-domains.[26]

A review of the thermoelectric materials developed to date indicate that some of these materials are toxic and many of them are based on the elements with low abundance in Earth's crust such as tellurium (Te), antimony (Sb), germanium (Ge), ytterbium (Yb), bismuth (Bi), selenium (Se), silver (Ag), and gallium (Ga). In comparison, most metal silicide thermoelectric materials are benign and some of them such as Mg_2Si, $MnSi_x$, $CrSi_2$, and β-$FeSi_2$ are made of elements with high crustal abundance. Transition metal silicides (TM) have especially achieved high Seebeck coefficients, which is often associated with the d-band states of the TM element.

Most metal silicides have appropriate melting temperature and bandgap for medium temperature power generation applications. The most favorable silicides include Mg_2Si, $MnSi_x$, $CrSi_2$, β-$FeSi_2$, and $ReSi_{1.75}$. In particular, the compounds of Mg_2X^{IV} (where X^{IV} = Si, Ge, and Sn) and their solid solutions have been of interest in recent studies[27–30] due to their demonstration of high zTs in medium temperature range comparable to some of the good thermoelectric materials such as lead telluride. Their abundance in nature and non-toxic features make them even more attractive, which fuel ongoing efforts to enhance their thermoelectric properties via different techniques such as nanostructuring. Nanostructuring has already shown zT improvement for silicides of germanium (germanium silicide is often referred to as silicon germanium). In the Si CMOS world, silicides are also widely used as low-resistivity contact and interconnect materials and the term germanosilicide is used for compounds of SiGe and metals such as Ti, Co, Ni, and Pt.[31–33] However, as we will discuss, nanostructuring is not very effective for the case of Mg_2Si due to the small difference of the phonon and electron mean free paths in this material. Therefore, other methods, such as band engineering have been pursued to improve the power factor. In particular, Sb doped $Mg_2Si_{0.4}Sn_{0.6}$ has shown $zT \sim 1.1$ at 800 K, which is comparable to the zT of PbTe.

Silicon germanium ($Si_{1-x}Ge_x$) and ruthenium silicide (Ru_2Si_3) are both good candidates for high temperature applications. Silicon germanium ($Si_{1-x}Ge_x$, $0.15 < x < 0.3$) is the only non-metal silicide, which has good thermoelectric properties. At higher temperatures (~1300 K), it has a fairly large Seebeck coefficient (>200 μV/K) and low thermal conductivity (<5 $W\,m^{-1}\,K^{-1}$), both resulting from the material's relatively large bandgap (~0.9 eV). The good thermoelectric properties and high melting temperature has made

germanium silicides appropriate for high temperature power generation applications such as radioisotope thermoelectric generators (RTG) used in spacecrafts. Nanostructured $Si_{1-x}Ge_x$ has shown enhanced zT both for p- and n-type materials.[34] Ru_2Si_3 also has good thermoelectric properties and can be potentially better than $Si_{1-x}Ge_x$ at high temperatures if it could be doped to the optimum carrier concentration, which has been historically challenging.[35]

Silicide nanocomposite engineering is another interesting direction that has been recently pursued. While the high frequency phonons are strongly scattered by point defects in alloys, the scattering of the low frequency phonons can be significantly enhanced resulting in even smaller thermal conductivity in nanocomposites consisting of nanoinclusions. The electrical conductivity is not significantly affected as the electron scattering by ionized impurities or acoustic phonons is usually more dominant than the scattering due to nanoinclusions. The addition of silicide nanoinclusions to the $Si_{0.88}Ge_{0.12}$ alloy maintained or increased the power factor while further reduced the thermal conductivity compared to the nanostructured single phase alloy. This resulted in zT enhancements in both $Si_{0.88}Ge_{0.12}$–$FeSi_2$[36] and $Si_{0.88}Ge_{0.12}$–Mg_2Si[37] nanocomposites reaching $zT \sim 1.2$ and 1.3, respectively, at 1200 K. These results confirmed the importance of nanostructuring in germanium silicide alloys proposed earlier by Mingo et al.[38] suggesting a new approach for making efficient thermoelectric materials.

2. Overview of silicide thermoelectrics

Since Nikitin[39,40] came up with the idea of using silicides as thermoelectrics in 1958, different silicides have been studied for mid- and high-temperature applications.[41] Among these materials, silicon germanium (SiGe) has been the best material for high temperature applications such as in RTGs used in spacecrafts for deep space science exploration.[42,43] Extensive theoretical and experimental studies have been carried out for the material system.[34,44–48]

SiGe alloys used to synthesize the first silicides used in RTGs were initially made by zone leveling and Czochralski techniques in 1960's. Boron and phosphorus (or arsenic) were used as the p- and n-type dopants, respectively. The solid solubility limit of these dopants are very small at room temperatures.[49] Accordingly, during measurement of the thermoelectric properties from room to high temperature, transport properties of heavily doped p- and n-type alloys alter with time due to the precipitation of dopants in SiGe lattice or grain boundaries.[50] To avoid loss of active dopants in heavily doped n-type alloys, the samples were annealed at ~925 °C, then, quenched to room temperature. Furthermore, they were measured from room temperature to 325 °C (metastable condition), then, they were measured as quickly as possible at higher temperatures. In p-type alloys with hole concentrations exceeding 3×10^{20}, precipitation happened only above 825 °C. The behavior of zT for both p- and n-type materials used in RTGs were similar, except that the maximum zT for n-type SiGe alloys was 30% more than the p-type alloys. The actual efficiency of the RTGs over the temperature range of 27–925 °C was 10% for the best developed samples.[51]

Many silicide compounds are considered as potential thermoelectric materials. The most well-known and applicable silicides are those of $Si_{1-x}Ge_x$ which have already demonstrated excellent thermoelectric properties. $Mg_2(Si,Sn)$ and $MnSi_{1.7}$ are also considered as highly promising silicides. In addition to these silicides, $ReSi_2$, $CrSi_2$, WSi_2, and $MoSi_2$ have large effective masses as well as high mobility along with low thermal conductivity, which make them potentially interesting candidates for RTGs. However, since the bandgaps of these materials are typically too small to prevent thermal excitation of the minority carriers, they suffer from bipolar transport at high temperatures for any doping concentration, which results in a low zT.[52]

In transition metal silicides, electrons in d-orbitals change the transport properties and bonding characteristics of the materials compared to s- and p-bonded compounds.[53] The d-band state results in a high Seebeck coefficient (150–200 μV/K) in silicides such as β-$FeSi_2$ and $MnSi_x$.[54]

Metal silicides are divided into different groups as follows: Group IA and IIA (alkali and alkaline earth) silicides are mostly semiconductors with bandgaps in the range of 0.5–1.3 eV. NaSi, Mg_2Si, Ca_2Si, $BaSi_2$, and Sr_2Si belong to these two groups. All these compounds can easily oxidize due to high chemically reactivity of the alkali and alkaline earth metals and need special handling. Group IIIB and rare earth (Sc, Y, and La–Lu) silicides have mostly metallic properties except α-$LaSi_2$ which has semiconducting properties. Group IVB (Ti, Zr, and Hf) silicides and group VB (V, Na, and Ta) silicides also have metallic properties. Group VIB (Cr, Mo, and W) silicides are all semiconductors and they have the potential to serve as thermoelectric materials. Group VIIB (Mn and Re) silicides are also semiconductors and they are widely used in thermoelectric applications. Group VIIIB (Fe, Ru, and Os) silicides too are semiconductors; of these, β-$FeSi_2$ is one of the most inexpensive silicides available.[53] Ru_2Si_3 can theoretically be a better thermoelectric material than SiGe at high temperatures. However, the lack of appropriate dopants and scarcity of Ru resources are the main obstacles of using this material.[54] Group IXB (Co, Rh, and Ir) silicides are not considered as good thermoelectric materials. Group XB (Ni, Pd, and Pt) silicides are all metallic compounds with no applications in thermoelectrics.[53] Group XIB (Cu, Ag, and Au) silicides are also not considered as potential thermoelectric materials. Cu and Si yield several intermetallic phases.[55] Ag has a eutectic point with Si.[56] Au is used for metallization of Si. Au and Si gives a very low eutectic point and all of the crystalline compounds are metastable.[57] Group XIIB (Zn, Cd, and Hg) silicides are also not considered in thermoelectrics mainly due to negligibly small solubility of Zn, Cd, and Hg in Si.[58–60]

In summary, metal silicides of β-$FeSi_2$, $CrSi_2$, $MnSi_{1.75}$, $Mg_2(Si,Sn)$, Ru_2Si_3, and $ReSi_{1.75}$, along with those of SiGe are the most promising thermoelectric silicides. These materials are appropriate for mid (300–600 °C) and high (over 600 °C) temperatures, which are within the range of waste heat in most industries.[61]

3. Traditional silicide thermoelectrics

Throughout the thermoelectric history, two different approaches were adopted to improve the zT figure-of-merit; reducing the thermal conductivity and/or improving the power factor. Introduction of particles of a second phase

in the alloy was initiated using gallium phosphide (GaP) incorporation into SiGe by Pisharody in 1978.[62] This resulted in 40–50% reduction of the thermal conductivity in both n- and p-type materials and improved zT in SiGe silicides. Another influential work was performed by Rowe[63] in 1974, which introduced fine grained SiGe in which, grain boundary scattering of phonons resulted in a reduced thermal conductivity.[64–66] This work inspired a series of new studies on SiGe.[36–38,44,46,47,67]

Despite the fact there is no theoretical limit for zT, the maximum zT of the state-of-the-art thermoelectric materials such as SiGe and $(Bi,Sb)_2(Se,Te)_3$ remained near unity for several decades.[68] In order to make thermoelectric systems with efficiencies comparable to the current technologies such as mechanical engines, it is highly desirable to have $ZT > 1.5$ for power generation and $ZT > 2$ for cooling[68–71] (here ZT refers to the device figure-of-merit, which includes parasitic losses due to electrical and thermal resistances). Furthermore, thermoelectric materials should be inexpensive, robust, non-hazardous and environmentally friendly for waste heat recovery applications.

Different strategies have been used to improve the zT figure-of-merit, such as using compounds of heavy element, complex crystal structures, point defect scattering, and resonant doping.[70] Until early 1990s, the maximum reported zT was ~1 and the energy conversion efficiency could not pass 10%, which restricted the application of thermoelectrics for spacecraft and electronic cooling.[52,72–74] In the last two decades, discovery of new thermoelectric materials along with nanostructuring techniques have continuously improved zT for several compounds.[3–10,36,37,75] These improvements inspired new applications with particular emphasis on waste heat recovery at different industries,[76,77] and to some extent for solar thermoelectric generators.[78] In addition, the National Aeronautics and Space Administration (NASA) is interested in high performance thermoelectric materials to improve the conversion efficiencies of their RTGs for the next generation space science missions.[79,80] In an RTG, even a small improvement in the thermoelectric properties of the materials while maintaining lifetime and reliability results in large amounts of energy savings. This is specially desired for multi-year planetary exploration spacecrafts such as Galile and Voyeger.[52]

4. Recent prospective

4.1 Nanostructured thermoelectrics

Since early 1990s, two approaches were followed to realize the next generation thermoelectric materials. The first approach relies on employing new bulk materials with low thermal conductivity and/or high power factor. The other approach focuses on engineering the microstructure to benefit from low-dimensional size effects.[11,81]

There have been quite a few successes in achieving enhanced zT in nanostructured n- and p-type SiGe.[44,46,47] However, nanostructuring did not show significant zT enhancement in other silicide alloys such as $MnSi_{1.7}$,[82] Mg_2Si,[83,84] or $FeSi_2$.[85,86]

Phonon scattering in bulk thermoelectric materials happens in several ways including phonon–phonon scattering, phonon–electron scattering, and phonon–point defect scattering. In $Si_{1-x}Ge_x$ alloys, point defect scattering is dominant for short wavelength phonons, whereas phonon–electron scattering is dominant for long wavelength phonons. It should also be noted that nanostructured thermoelectrics are generally highly doped to achieve the peak zT. Therefore, the phonon–electron scattering can be significant reducing the thermal conductivity especially at low temperatures. Bulk nanostructuring produces a high density of two-dimensional defects such as interfaces and grain boundaries as well as nano-scale particles along with point defects. Consequently, due to the broad distribution of the size of the defects, phonon scattering can happen at both short and long wavelengths.[80] The interfaces can have a secondary effect in improving the zT. Due to the preferential scattering of low energy (long wavelength) charged carriers at interfaces, the Seebeck coefficient in nanostructured thermoelectric materials is usually higher than that of the crystalline material at similar doping concentration. In addition, since the minority carriers will have a smaller energy than majority carriers, they are scattered more strongly at interfaces leading to lower bipolar transport, which explains the higher effectiveness of nanostructuring at high temperatures.[44,87]

4.2 Nanocomposite approach

Nanocomposite refers to a class of materials that are made of more than one phase. It can be made of different phases of the same material, such as amorphous–crystalline nanocomposites, or it can be made of different materials. Nanocomposites, like nanostructured single phase materials, can have a lower thermal conductivity than the "alloy limit".[18] They may also have a larger power factor than the constituent phases. Although a classical composite material cannot have higher zT than each of the constituent phases,[88,89] the nano-scale effects in nanocomposites can result in zT improvement. For example, high zT has been obtained in several thermoelectric nanocomposites such as InGaAs/ErAs,[18,90] PbTe–SrTe,[47] SiGe–$CrSi_2$,[91] and BiSbTe.[23] In another related approach, Mingo et al. predicted enhanced zT in nanocomposites made of silicide nanoparticles in SiGe alloys[38] and several follow-up studies further confirmed this prediction.[36,37]

A review of the properties of the best reported silicide thermoelectric materials is presented in the following sections. However, the reader should note that due to the complexity of the measurements, the measured zT values may include a significant error. Even with today's commercially available equipment for measuring the electrical conductivity, Seebeck coefficient, and thermal conductivity, the deducted zT can be off by as much as 20%.[92] Besides, improper sample geometries can further increase the tolerance. Such a tolerance should be taken into consideration when comparing the zT values reported from different laboratories; hence, small zT improvements may be within the measurement variations. Unfortunately, some commercial equipment of the Seebeck coefficient and electrical conductivity measurement do not eliminate the residual voltage at zero temperature gradient (a.k.a. dark EMF) in the calculation of the Seebeck coefficient and result in erroneously large Seebeck values. Such measurements may also result in large estimation of the zT values. It should be noted that considering only the maximum zT as an indication of the thermoelectric material excellency is not accurate as one must also consider the average zT over the working temperature.[93]

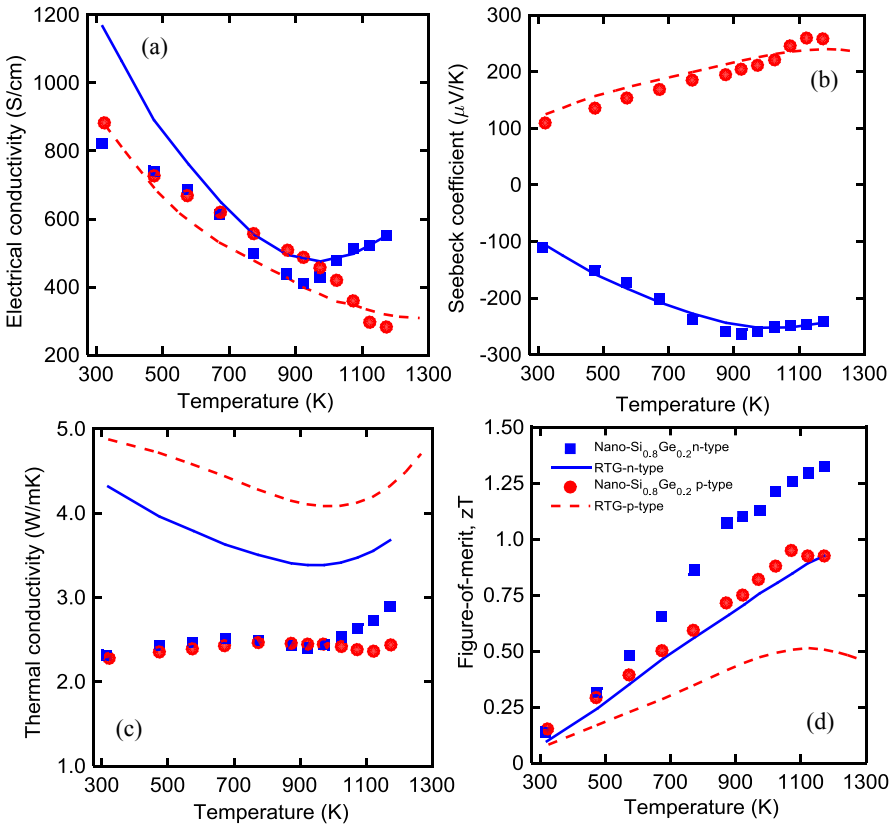

Fig. 1. (Color online) (a) Electrical conductivity, (b) Seebeck coefficient, (c) thermal conductivity, and (d) zT of n- and p-type nanostructured bulk $Si_{0.8}Ge_{0.2}$ samples compared with those of the n- and p-type RTG reference sample. Ref: n-type $Si_{0.8}Ge_{0.2}$[47] and p-type $Si_{0.8}Ge_{0.2}$.[46]

The data reported here is taken from the literature. In some cases, a missing material property, wherever possible, was estimated from the reported material properties, e.g., electrical conductivity from the plotted Seebeck coefficient and the power factor.

5. Silicon germanium (SiGe)

SiGe is a widely used thermoelectric material for high temperature applications such as RTGs.[94] Germanium is added to silicon to decrease the thermal conductivity significantly without sacrificing the electrical conductivity. Consequently, the zT value of the SiGe alloy material can be significantly increased compared to Si. In order to improve the performance of the SiGe material, much research has been done so far which is briefly summarized here.

5.1 Crystalline and polycrystalline SiGe

Back in 1964, the thermal and electrical properties of SiGe alloy were studied by Dismukes.[51] The maximum zT of n- and p-type $Si_{0.7}Ge_{0.3}$ was measured to be about 1 and 0.7, respectively. At the early stage of the SiGe study, the main technique employed to improve the zT was boundary scattering of phonons. Goldsmid and Penn presented this idea in 1968.[95] They pointed out the thermal conductivity of the material can be decreased by boundary scattering even when the sizes of the crystals are much larger than the phonon mean free path. It was believed that the electrical conductivity will not be affected since in highly doped SiGe the electron mean free path is much smaller than the phonon mean free path. In 1981, Rowe et al. reported the first experimental results of fine grained hot pressed compacts of heavily doped n-type SiGe.[65] The results showed that when the grain size is smaller than 5 μm, the thermal conductivity can be decreased by 28% compared with single crystal SiGe. Later, Vining et al. demonstrated pressure-sintered $Si_{0.8}Ge_{0.2}$ with particle sizes ranging from 1 to 100 μm.[96] The results showed that the thermal conductivity can be significantly reduced by 50% with particle sizes around 2 μm. However, the improved zT values were not observed. The maximum zT of pressure-sintered n- and p-type $Si_{0.8}Ge_{0.2}$ was measured to be about 1 and 0.6. The authors claimed that this is due to the reduction of the electrical conductivity.

5.2 Bulk SiGe nanocomposites

There was little progress for SiGe thermoelectric materials research from 1960s to 1990s; the zT values were limited to ~1 and ~0.7 for n- and p-type SiGe, respectively. However, during the past twenty years, significant progresses were achieved by employing nanostructured bulk of SiGe. In 2008, Wang et al. reported a peak zT value of 1.3 at 1173 K for n-type nanostructured bulk SiGe alloy.[47] $Si_{0.8}Ge_{0.2}$ was fabricated by hot pressing from ball milled Si, Ge chunks and P micro-powders. The grain size of the material was measured to be 10–20 nm. At this grain size level, the phonon scattering was significantly increased and the thermal conductivity was greatly decreased. The Seebeck coefficient and high temperature electrical conductivity did not change noticeably compared to that of RTG alloy. As a result, the zT value of the nanostructured bulk SiGe was effectively improved as shown in Fig. 1.

P-type nanostructured bulk SiGe alloy with a peak zT value of 0.95 at 900–950 °C was also reported by Joshi et al.[46] Employing the hot pressing and ball milling technique, the boron doped nanostructured bulk SiGe with

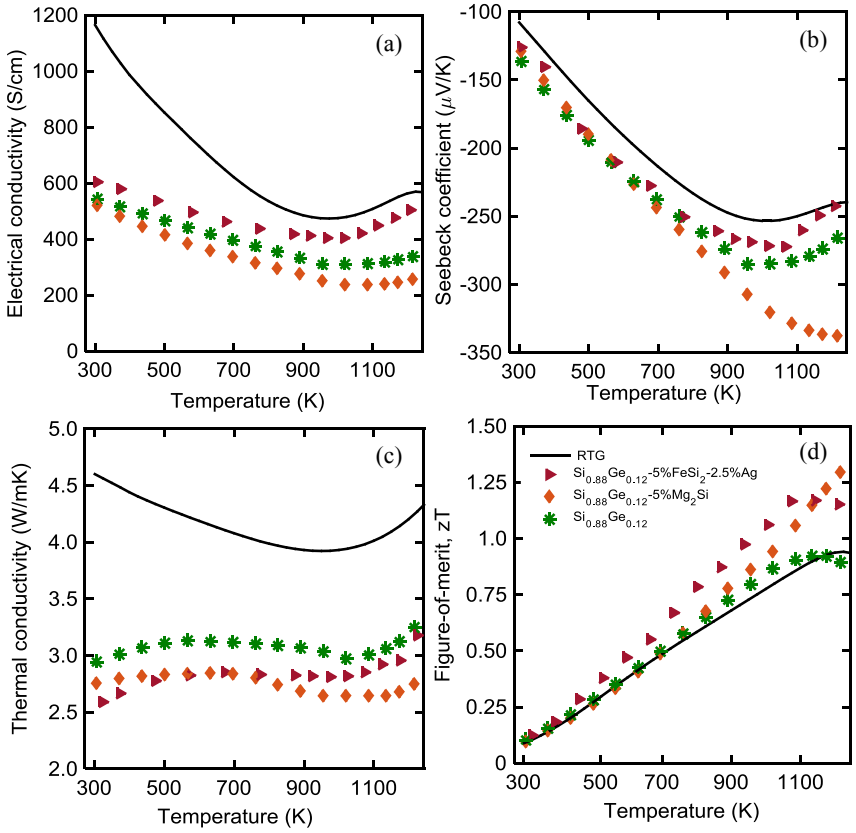

Fig. 2. (Color online) (a) Electrical conductivity, (b) Seebeck coefficient, (c) thermal conductivity, and (d) zT of nanocomposites of SiGe–$FeSi_2$ and SiGe–Mg_2Si in symbols. The solid line shows the data of the RTG sample. Ref: SiGe–$FeSi_2$[36] and SiGe–Mg_2Si.[37]

grain sizes ranging from 5 to 50 nm was obtained. Similar to the n-type counterpart, the improvement of the zT value was mainly due to the significant decrease of the thermal conductivity as shown in Fig. 1.

5.3 Effect of nanoinclusions

In 2009, Mingo et al. introduce the idea of a nanocomposite SiGe material based on silicide nanoparticles embedded in a SiGe alloy matrix.[38] According to the modeling results, at room temperature, a potential 5-fold increase in zT was predicted, which is ~0.5; and at 900 °C, a potential 2.5-fold increase in zT was predicted, which is ~1.7. The main reason for zT enhancement was due to reduction of thermal conductivity via phonon scattering by the nano-inclusions. Furthermore, as discussed, the silicide nanoinclusions may improve the thermoelectric power factor through preferential scattering of the low energy charge carriers. Experimental results showed that Mg_2Si–$Si_{0.88}Ge_{0.12}$ and $FeSi_2$–$Si_{0.88}Ge_{0.12}$ nanocomposites have smaller thermal conductivity compared with nanostructured $Si_{0.8}Ge_{0.2}$. In these materials, the Seebeck coefficient increased and the electrical conductivity decreased resulting in almost similar power factor compared to that of RTG SiGe alloy. Therefore, the reduction of thermal conductivity resulted in higher zT (Fig. 2).[36,37] This also allowed reducing the amount of germanium from 20 to 12% in the alloy, which reduces the materials cost, while still improving the zT.

In another study, cost-effective fabrication of n-type SiGe–$FeSi_2$ nanocomposite was studied.[97] The cost was optimized by using low purity components, especially oxidized germanium powder, and utilizing induction melting over mechanical alloying for obtaining a uniform alloy in much shorter time. Furthermore, the effect of addition of carbon for oxide reduction was studied and a high zT of 0.8 was achieved around 1200 K.

5.4 Low-dimensional SiGe

Besides bulk nanostructuring, low dimensional structures, such as nanowires and superlattices, were employed to improve the zT of SiGe. In one and two-dimensional materials, the phonon scattering is enhanced due to the boundaries of the low-dimensional structure. Martinez et al. studied the thermal and electrical properties of an individual p-type SiGe nanowire for the first time.[98] Thermal conductivity of the nanowire was effectively decreased due to the phonon scattering at the wire boundaries. The zT value of the nanowire was improved by a factor of 2 compared to single crystal counterpart. Later, Lee et al. demonstrated n-type SiGe nanowires with an improved zT of 0.46 at 450 K.[99] In this study, SiGe nanowires with diameters ranging from 26 to 161 nm were grown by vapor–liquid–solid (VLS) method. The authors also predicted zT values higher than 2 at 800 K using theoretical simulations based on Boltzman transport equation.[99] For two-dimensional superlattices, early in 1997, Lee presented a thermal conductivity study on two-dimensional SiGe superlattices.[100] The thermal conductivity of the n-type SiGe superlattice was decreased to 1–2 $W\,m^{-1}\,K^{-1}$ at temperatures up to 500 K. Recently, Samarelli demonstrated Ge/SiGe modulation doped superlattices with enhanced power factor and zT value at room temperature compared to Ge and $Si_{1-y}Ge_y$ materials.[101]

5.5 Thermal conductivity of SiGe: Lowest value

There has been much effort to find techniques for suppressing the thermal conductivity of SiGe and improving the zT. It is

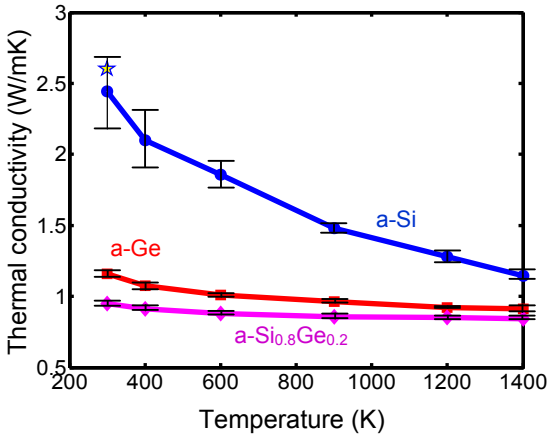

Fig. 3. (Color online) Calculated thermal conductivity of amorphous silicon, germanium and $Si_{0.8}Ge_{0.2}$. Reproduced from Ref. 103.

important to know how far the thermal conductivity can be reduced. Lee et al. investigated the theoretical limit of the thermal conductivity of SiGe alloys.[102] In this work, the authors discovered that the thermal conductivity is strongly related to the size of the random alloy unit cell in their study. The theoretical analysis of the thermal conductivity converged to a minimum around 1–2 $W\,m^{-1}\,K^{-1}$ for the composition of $Si_{0.8}Ge_{0.2}$.

In another computational study, Norouzzadeh et al. analyzed the thermal conductivity of amorphous $Si_{1-x}Ge_x$ compound versus x and temperature, which sets the minimum thermal conductivity achievable by nanostructuring and compositional change of $Si_{1-x}Ge_x$.[103] Although amorphous SiGe suffers from low electrical conductivity, the thermal conductivity can reach the lower limit since the lattice is fully disordered. Figure 3 illustrates the calculated thermal conductivity of amorphous silicon, germanium and $Si_{0.8}Ge_{0.2}$ versus temperature. It is shown that the thermal conductivity of the amorphous $Si_{0.8}Ge_{0.2}$ is less than 1 $W\,m^{-1}\,K^{-1}$ with small reduction as the temperature increases from 300 to 1400 K.

6. Magnesium silicide (Mg_2Si) alloys

Mg_2Si and CaMgSi are promising candidates for thermoelectric materials due to the natural abundance and nontoxicity of the constituent elements, low material density, and tailorable electronic structure.[83] Mg_2Si is a semiconductor with an indirect bandgap of 0.61 eV at 300 K (0.69 eV at 4 K).[104] Due to its high Seebeck coefficient and low thermal conductivity, Mg_2Si was initially thought to be a good candidate for nanostructuring to improve zT. For some materials such as $Si_{1-x}Ge_x$, zT was significantly enhanced by producing a nanostructure with grain sizes smaller than the mean free path of broad range of phonons and larger than the mean free path of charge carriers. This turned out not to be the case for Mg_2Si as the losses in electrical conductivity due to a significant decrease of mobility largely negate the beneficial effects of decreased lattice thermal conductivity and slightly improved Seebeck due to the carrier filtering effect.[84] Due to these difficulties, other strategies for improving the efficiency of these materials are being explored such as alloying, carrier pocket engineering, and incorporation of different dopants.

Sb is the preferred electron donor for n-type doping of this material. A co-doping scheme using Ge and Sb produced a maximum zT value of 0.74 at 756 K for n-type material, while material not containing Ge had a maximum zT value of ~0.5, as shown in Fig. 4.[105] The working principle is that point defects decrease the lattice contribution to thermal conductivity by scattering short wavelength phonons, so while Ge addition caused a moderate decrease in mobility, this was outweighed by a significant decrease in thermal conductivity and improvement in Seebeck coefficient at high Sb doping which contributed to a significant enhancement in zT. The high electrical conductivity due to Sb doping also increased the thermal conductivity due to the enhancement of the electronic thermal conductivity.

Mg_2Si performance can be greatly improved by alloying with Mg_2Sn. An n-type composition of $Mg_{2.15}Si_{0.28}Sn_{0.71}Sb_{0.006}$ achieved a zT value of over 1.3.[106] The power factor enhancement was assumed to be the result of the convergence of the heavy and light conduction bands at this composition. This band convergence increases the power factor by enhancing the density of states effective mass by adding carrier pockets near the band edge, which serves to increase the magnitude of the Seebeck coefficient for a given carrier concentration. Also due to a decrease in bandgap resulted from alloying, or the reduction of the Fermi energy due to larger density of states near the band edge, the onset of the bipolar carrier effects caused the maximum zT to occur at ~700 K, while for doped Mg_2Si such effects were not apparent until ~800 K.

One issue that hinders the use of Mg_2Si materials is the lack of a comparable p-type material that demonstrates similar performance in the same temperature range. Ag-doped materials exhibit $zT \sim 0.11$, which is over an order of magnitude lower than the best n-type materials.[108] Without a well matched p-type material, it is impossible to achieve optimum performance in a traditional thermoelectric device. Several possibilities for improving p-type performance have been used, mainly trying to find dopants that are more easily activated (shallow acceptor states) and can produce the optimum carrier concentration in the valence band for similar high temperature performance to the n-type materials.

Figure 5 shows the reported zT of several Mg_2Si alloys doped with different elements. Improvements in zT due to alloying with Ge are apparent for Ga-doped materials. Ga-doped (0.8 at. %) Mg_2Si has a maximum $zT < 0.13$ at 650 K. With the same level of Ga doping, $Mg_2Si_{0.6}Ge_{0.4}$ has a maximum zT of ~0.36 at 623 K. Ga-doping decreased the lattice thermal conductivity, but the samples with Ge had roughly twice the carrier concentration at similar doping levels. Significantly lower thermal conductivity at all temperatures and an improved Seebeck coefficient at high temperatures lead to significantly improved material performance.

A similar composition to the n-type Mg_2Si–Mg_2Sn alloys, which exhibited enhanced $zT \sim 0.5$, was $Mg_{1.86}Li_{0.14}Si_{0.3}Sn_{0.7}$ in which Li was doped as an acceptor.[109] Li was assumed to substitute for Mg in the alloy crystal structure, but the degree of ionization of Li was estimated to be no more than about 30% (~30% of Li atoms contributed holes to the crystal). The alloy composition was designed using relatively simple modeling to engineer a band structure which has a low

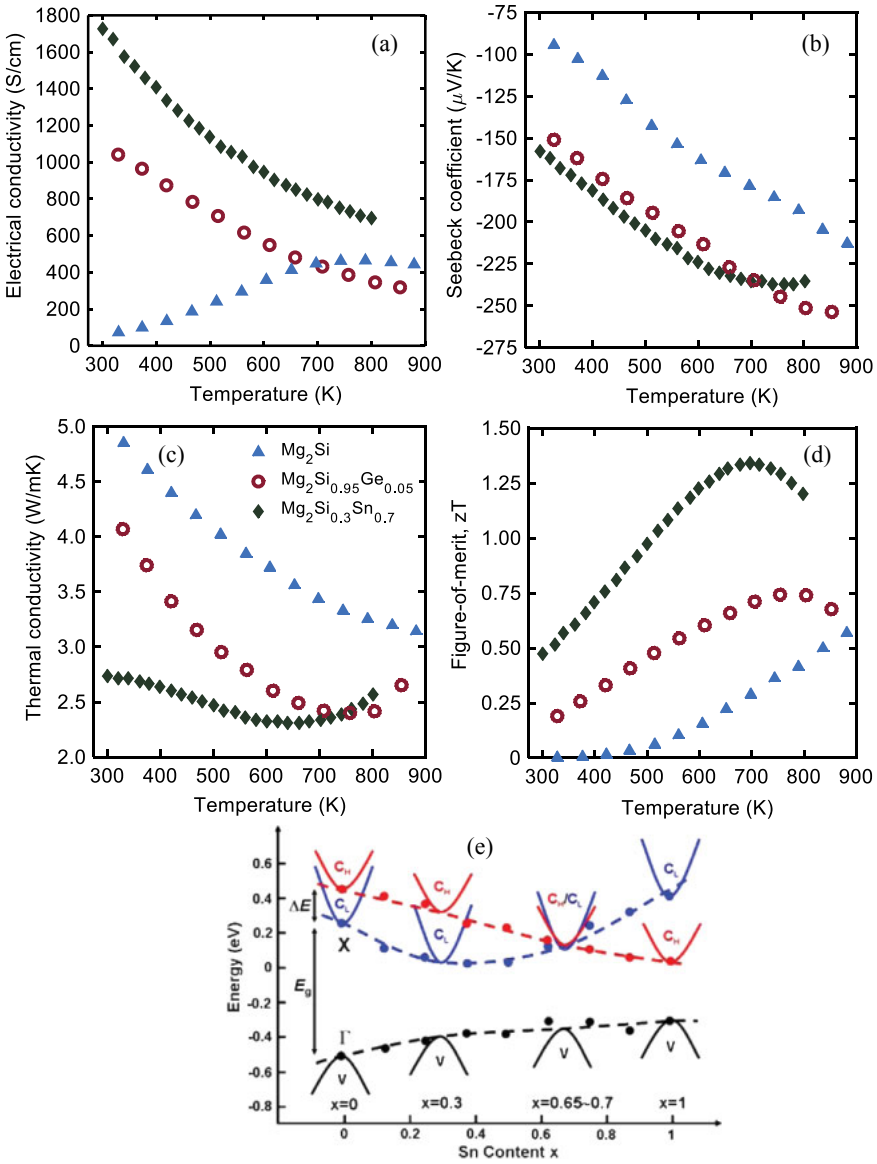

Fig. 4. (Color online) (a) Electrical conductivity, (b) Seebeck coefficient, (c) thermal conductivity, and (d) zT versus temperature for selected compositions of n-type Mg_2Si alloys, all of which are doped with Sb. Ref: Mg_2Si,[107] $Mg_2Si_{0.95}Ge_{0.05}$,[105] and $Mg_2Si_{0.3}Sn_{0.7}$.[106] (e) The highest valence band and the comparative location of the light and heavy conduction bands for $Mg_2Si_{1-x}Sn_x$ as a function of Sn content. The red dashed line shows energy variation of heavy conduction band versus Sn content. The blue and black dashed lines show change of the light conduction band and valance band, respectively. The solid dots describe the calculated data for various Sn content.[106]

density of states near the Fermi level and a large slope of density of states per unit energy. The significantly higher onset temperature for the decrease in zT from bipolar effects also indicated more successful doping than other p-type materials.

As another p-type candidate based on Mg_2Si system, CaMgSi intermetallic phase is thought to be a promising one due to lower electrical resistivity compared to Mg_2Si and high positive Seebeck coefficient estimated at 750–900 μV/K for intrinsic type material.[110] Further studies of thermal and electrical transport properties and doping still need to be assessed to determine the effectiveness of this material as a thermoelectric.

7. Manganese silicides ($MnSi_x$)

Manganese silicides ($MnSi_x$) with x ranging from 1.71 to 1.75,[94] also known as higher manganese silicides (HMS), are made up of complex chimney-ladder structures with tetragonal cells. HMS forms with a variety of compositions such as Mn_7Si_{12},[111] $Mn_{11}Si_{19}$,[112,113] $Mn_{26}Si_{45}$,[111] $Mn_{15}Si_{26}$,[114,115] $Mn_{19}Si_{33}$,[111] $Mn_{27}Si_{47}$,[116] $Mn_{39}Si_{68}$,[111] and Mn_4Si_7.[117] HMS crystals consist of regions of homogenous composition separated by regions of abrupt phase transitions. These transition regions are generally composed of manganese monosilicide (MnSi). The MnSi precipitate layers are formed perpendicular to the C-axis and are independent of growth technique. In undoped HMS the precipitate layers are around 1 μm thick separated by a distance of 10–120 μm.[118] These MnSi precipitates act as energy barriers and can influence the transport properties of the charge carriers. HMS naturally is a p-type semiconductor with a carrier concentration of 10^{21} cm^{-3} and a carrier mobility of ~10 cm^2 V^{-1} s^{-1} at 300 K. $Mn_{11}Si_{19}$ has an indirect band gap with absorption edge energy of approximately 0.64 eV at 5 K.[119] The monocrystals

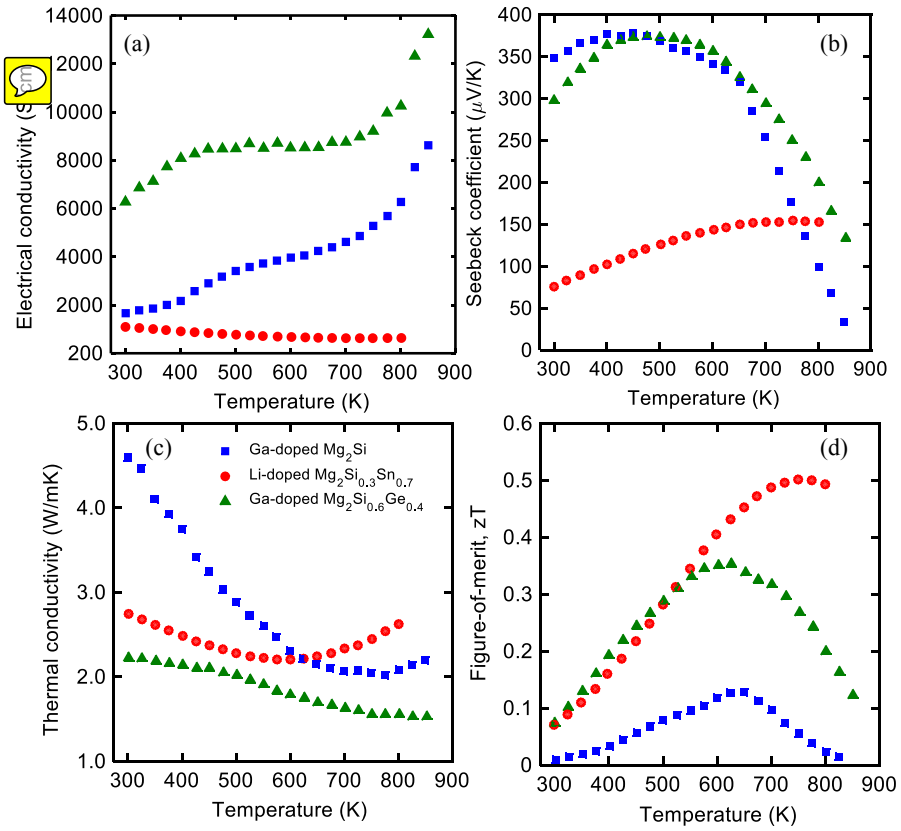

Fig. 5. (Color online) (a) Electrical conductivity, (b) Seebeck coefficient, (c) thermal conductivity, and (d) zT values for different p-type Mg_2Si materials. Refs: Ga-doped Mg_2Si,[108] Ga-doped $Mg_2Si_{0.6}Ge_{0.4}$,[108] and Li-doped $Mg_2Si_{0.3}Sn_{0.7}$.[109]

of HMS exhibit anisotropy in Seebeck coefficient. The ratio of Seebeck coefficient between perpendicular and parallel direction to the C-axis can be ~1.7. Similarly, the ratio of electrical conductivity and thermal conductivity between perpendicular and parallel direction to the C-axis is 5 to 170 and 2, respectively at 300 K.[43] Therefore, polycrystalline HMS is preferred if isotropic properties are desired.

Norouzzadeh et al.[82] have used a two-band semi-emperical model to explain and compare the thermoelectric properties of bulk and nanostructured phase of HMS phase. They were able to show that the nanostructuring does not significantly improve the zT of HMS, which can explain why there has not been much success in improving its zT by bulk nanostructuring. This was due to the significant decrease in electrical conductivity as a result of increased electron scattering at the grain boundaries. Band structure engineering was, therefore, recommended as a more efficient approach than nanostructuring to improve its zT.

Apart from thermoelectric properties, HMS alloys are also mechanically robust, inexpensive, non-toxic and highly resistant to oxidation. HMS samples prepared by different techniques show zT of around 0.3–0.5. Different approaches such as nanostructuring, Mn and Si substitution and nanoparticle inclusion have been used to improve the thermoelectric properties of HMS, which are briefly discussed below.

Synthesis: The most common way to synthesize HMS is to perform induction melting or mechanical alloying of the elemental powders of Mn and Si of the desired stoichiometry followed by spark plasma sintering (SPS) or hot pressing (HP). Zamanipour et al.[120] studied the thermoelectric properties of different nanostructured phases of HMS prepared by mechanical milling (50 h) and hot pressing (950 °C for 5 min). Out of the phases studied $MnSi_{1.75}$ displayed the best thermoelectric properties with a maximum zT of 0.55 at 600 °C. However, the nanostructuring of the material resulted in only a small improvement of its zT.

A comparison has been performed between wet and dry milling for synthesis of HMS by Truong et al.[121] Wet milled material showed better thermoelectric properties with higher Seebeck and lower thermal conductivity. This was attributed to the finer particle size achieved by wet milling compared to dry milling which was limited due to the welding of particles during the dry mill. They also noticed the absence of the undesired MnSi phase after the wet milling process.

Ge substitution of Si in HMS has shown to improve the zT to 0.6.[122] According to this study Ge addition resulted in a decrease in thermal conductivity which can be attributed to the increase in phonon scattering due to the introduction of defects to the lattice structure. Al substitution, which introduced defects and increased the charge carriers, resulted in slightly higher zT of 0.65 at 527 °C[123] although such small changes of zT can be well within the measurement tolerances. In both cases, the optimal zT was at the solubility limits of the additives. In addition, different ratios of co-doped Al and Ge has been studied by Chen et al. which showed no improvement compared to Al doping.[124]

Alumina nanoparticles was also used to reduce the thermal conductivity.[125] This showed more reduction in thermal conductivity due to the increased phonon scattering by nanoparticles. However, the particle addition also resulted in a reduction of electrical conductivity. The best zT was again

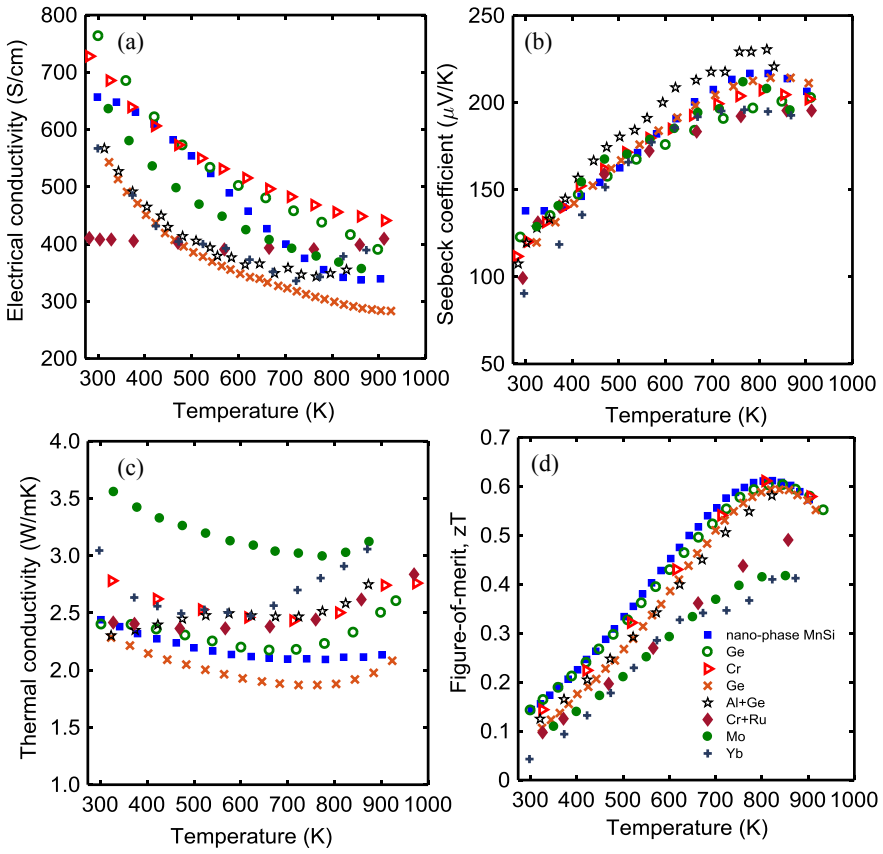

Fig. 6. (Color online) Comparison of (a) electrical conductivity, (b) Seebeck coefficient, (c) thermal conductivity, and (d) zT values of HMS prepared with different dopants. Refs: nano-phase MnSi,[126] Ge-doped,[132] Cr-doped,[133] Cr+Ru-doped,[133] Ge-doped,[122] Al+Ge-doped,[124] Mo-doped,[134] and Yb-doped.[135]

~0.59 at 527 °C, which was obtained for HMS with 1% alumina.

Luo et al. have shown improvements in zT by adding MnSi nano-inclusions resulting from the process of melt spinning followed by SPS.[126] It is generally known that MnSi phase is detrimental to thermoelectric properties due to the small band gap and high conductivity, which results in a low Seebeck coefficient. MnSi nanoinclusion has resulted in decreased thermal conductivity which was attributed to the reduction of ambipolar diffusion due to energy dependent scattering of charge carriers.[127] Their process resulted in 50–100 nm MnSi particles and a peak zT of 0.62 at 527 °C.

Godke et al. showed that heavy atom substitution increases alloy scattering which can result in a reduction of lattice thermal conductivity. Chen et al.[128] explored this approach by using Re substitution of Mn.[129] A solid-state reaction followed by ball milling and SPS resulted in a maximum zT of 0.57 at 527 °C for $Re_{0.04}Mn_{0.96}Si_{1.8}$. The Re substitution resulted in an unchanged power factor but a reduced thermal conductivity. The amount of Re was limited by its solid solubility in HMS.

Yamamoto et al.[130] observed that addition of Re above the solubility limit resulted in production of large amounts of $ReSi_2$ as a secondary phase which decreased the power factor of the material. Recently, the solubility limit of Re was increased using a liquid quenching technique.[131] This resulted in a material with the high $zT \approx 1$ at 647 °C.[130]

Overall, different methods have been explored to improve the thermoelectric properties of HMS with most of these focused on reducing the thermal conductivity of the material. Nevertheless, the maximum zT remained persistently around 0.6. A comparison of zT of selected HMS materials with different dopants is represented in Fig. 6.

8. Chromium disilicide ($CrSi_2$)

Chromium disilicide ($CrSi_2$) has been of interest for thermoelectric applications because of its natural abundance, non-toxicity, good mechanical properties, oxidation resistance in air, and thermal stability at high temperature (up to 1000 K).[136]

$CrSi_2$ is a degenerate p-type semiconductor[137] with a hexagonal crystal structure, i.e., the so-called C40-type structure. It has a narrow indirect band gap of 0.35 eV.[138] $CrSi_2$ has significant anisotropy of Seebeck coefficient in a wide temperature range. However, its high thermal conductivity and a medium Seebeck coefficient result in a small zT with maximum value of 0.25 for the undoped material[139] as shown in Fig. 7. Compared with other silicides, $CrSi_2$ has high thermal conductivity, high electric conductivity, and medium Seebeck coefficient. Around room temperature, its zT value is higher than most other silicides.

Several methods have been employed to enhance the Seebeck coefficient and reduce the thermal conductivity including varying its stoichiometry, structural disordering and nanostructuring. $CrSi_2$ has been prepared by mechanical alloying and subsequent hot pressing like many other nanostructured bulk materials. For example, by decreasing the thermal conductivity and electric conductivity of $CrSi_2$ and $CrSi_{2.1}$, a modest incensement in zT (5% compared with un-milled $CrSi_2$) was observed in $CrSi_{2.1}$ alloy composi-

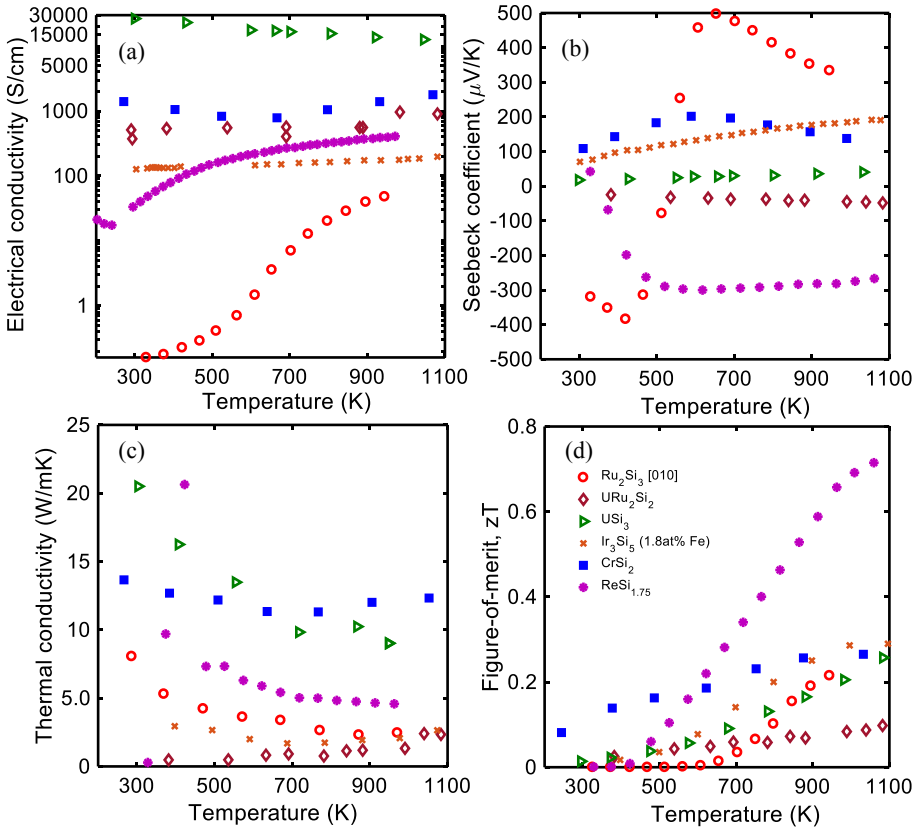

Fig. 7. (Color online) Comparison of (a) electrical conductivity, (b) Seebeck coefficient, (c) thermal conductivity, and (d) zT values of $CrSi_2$,[139] $ReSi_{1.75}$,[144] Ru_2Si_3,[146] URu_2Si_2,[147] USi_3,[148] and Ir_3Si_5.[151]

tion.[136] More recently, substitution of different elements have been studied. It was found that the maximum zT value for $Cr_{1-x}V_xSi_2$ was ~0.2 for $x = 0.08$ at 450 K due to the reduction of the thermal conductivity.[140] Mo substitution was also effective in improving the zT value. The maximum zT value of $Cr_{1-x}Mo_xSi_2$ increased from 0.13 to 0.23 for $x = 0.30$ at 800 K.[141] Nb substitution could reduce the thermal conductivity and increase the maximum zT by a factor of about 1.2 (0.20 in $Cr_{0.95}Nb_{0.05}Si_2$) relative to that of Nb-free $CrSi_2$.[142]

9. Rhenium silicide ($ReSi_{1.75}$)

It has been shown that higher rhenium silicide has the composition of $ReSi_{1.75}$ rather than previously thought $ReSi_2$. The crystal structure of $ReSi_{1.75}$ should be described as a triclinic (space group $P1$, $a = 0.3138$; $b = 0.3120$; $c = 0.7670$ nm; $\alpha = 89°90$).[143] One important feature of the band structure of $ReSi_{1.75}$ is that the highest valence band in the [001] direction is almost flat. This results in a very large hole effective mass, which explains the large anisotropy of the thermoelectric properties of $ReSi_{1.75}$. The value of electrical resistivity is higher along [001] than along [100]. Its electrical conduction is of n-type when measured along [001] while it is of p-type when measured along [100]. When measuring along [001], a large zT of 0.7 is achieved at 1073 K, as shown in Fig. 7. The zT value is further increased to 0.8 with a small amount of Mo addition (2% substitution for Re).[144] Compared with other silicides, $ReSi_{1.75}$ has small electrical conductivity, large Seebeck coefficient and zT along [001] direction. Its zT value at high temperature is significantly larger than many other silicides.

10. Ruthenium silicide (Ru_2Si_3)

Although Ru_2Si_3 has the disadvantage of being expensive, it is still considered to be a potential thermoelectric material for high temperature applications. Ru_2Si_3 is one of the family of related compounds Ru_2X_3 where X can be Si, Ge, or Sn. It has a high-temperature and a low-temperature phase. The phase transition happens at ~1240 K.[145] Low-temperature phase α-Ru_2Si_3 has an orthorhombic structure, whereas high-temperature phase β-Ru_2Si_3 has a tetragonal structure (a Nowotny chimney-ladder).[61] The α/β phase transformation is expected to have a significant effect on the use of Ru_2Si_3 as a thermoelectric material with greater interest in the α-phase.[146] Simkin et al.[146] performed floating-zone crystal growth of stoichiometric Ru_2Si_3 and measured the thermoelectric properties, which is shown in Fig. 7. The measured thermoelectric properties for the intrinsic (p-type) Ru_2Si_3 were clearly superior along the [010] orientation, consistent with the band structure models. Compared with other silicides, Ru_2Si_3 has small thermal and electric conductivity, and a medium zT.

11. Uranium ruthenium silicide (URu_2Si_2)

A large amount of uranium is discharged during a nuclear fuel cycle. The amount of depleted uranium is large and they cannot be reused for nuclear fuel. Therefore, uranium could be used for thermoelectric materials after about 50 years when they become non-radioactive. Since uranium has 5f-electrons, some uranium compounds are heavy fermion compounds, which can have a large effective mass of electron or hole.[147] This could result in a high Seebeck coefficient.

The thermoelectric properties of URu_2Si_2 were studied, as shown in Fig. 7.[147] A maximum zT of ~0.1 was reached at 1100 K in this study. The thermoelectric properties were poor above room temperature. However, since there has not been much study on this material, further optimization may be possible to improve it zT.

12. Uranium silicide (USi_3)

The high atomic mass difference in USi_3 should be in favor of a low thermal conductivity. Thermoelectric properties of USi_3 were studied as shown in Fig. 7. Compared with other silicides, USi_3 has low Seebeck coefficient, very high electric conductivity and a medium zT. $U(Si,Ge)_3$ solid solutions have been also studied, where they showed to be essentially metallic in nature reflected from their very high electric conductivity.[148]

13. Iridium silicide (Ir_3Si_5)

Ir_3Si_5 is a wide bandgap semiconductor with an optical gap of 1.56 eV,[149] which allows for applications at high temperatures. Its bulk material and single crystals were studied, but the zT value for the iridium silicides hardly exceeded 0.1.[150] Properties of semiconducting iridium silicide films have also been studied. Fe-doped iridium silicide films with high thermoelectric power factors were successfully obtained and the maximum zT reached ~0.3 when the amount of Fe dopant was 1.8 at. %,[151] as shown in Fig. 7, which is in the same order as some other silicides at high temperature.

14. Iron disilicide ($FeSi_2$)

Iron disilicide has three phases of ε-$FeSi_2$ (cubic), α-$FeSi_2$ (tetragonal), and β-$FeSi_2$ (orthorhombic). β-$FeSi_2$ is semiconductor and of interest for thermoelectric applications. It is a good candidate for thermoelectric applications due to low cost, non-toxicity and ease of fabrication. It is also chemically stable and has a sufficiently high figure of merit. Moreover, it has been combined with other high zT materials like SiGe[85] to form more efficient and cost-effective nanocomposites. β-$FeSi_2$ has a direct band gap of 0.80–0.95 eV and an indirect band gap of 0.7–0.78 eV,[152,153] which makes it a suitable option for making optoelectronic devices, light detector and photovoltaic applications.

14.1 $FeSi_2$: Properties and different phases

Iron disilicide has a metallic high temperature phase (α-$FeSi_2$) and a semiconducting low temperature phase (β-$FeSi_2$) with a transition temperature of about 1210 K. Undoped β-$FeSi_2$ single crystals obtained from very high purity starting material showed n-type conduction at room temperature.[154] Room temperature Seebeck coefficient of $-750\,\mu V/K$ and electrical resistivity of $230\,\Omega$cm was reported for pure β-$FeSi_2$ single crystals. It was suggested by Behr et al.[154] that the p-type conductivity for undoped $FeSi_2$ single crystals reported in literature occurs due to unintentional contamination by impure starting materials.

The high temperature metallic phase of the iron disilicide consists of a eutectic structure comprising cubic ε-phase and tetragonal α-phase. The ε-phase is an iron monosilicide FeSi, and the α-phase exists within a wide composition range, being represented by the chemical formula Fe_2Si_5. While the phase transition from semiconducting to metallic phase is fast, the phase transformation from metallic to semiconducting phase is slow and occurs in three stages. In the first stage, a peritectoid reaction occurs between α- and ε-phases to form the β-phase above 1138 K ($\alpha + \varepsilon \rightarrow \beta$). In the second stage eutectoid decomposition of α phases to β and Si occurs below 1133 K ($\alpha \rightarrow \beta + \mathrm{Si}$). In the third stage, remaining ε-phase reacts with Si to form the β-phase ($\varepsilon + \mathrm{Si} \rightarrow \beta$), completing the transformation through heat treatment.[155] This process takes several hours to complete due to slow reaction kinetics.

14.2 $FeSi_2$: Methods of fabrication

Since 1964, when iron disilicide was first suggested as a potential thermoelectric material by Ware and McNeill,[156] much work has been done to improve the properties and cost-effectiveness of this material. Different fabrication techniques have been employed to synthesize bulk or thin films of iron disilicide in the form of single crystalline, polycrystalline, nanostructured materials, or even nanocomposites. Recent advances in preparation of bulk and single crystal iron disilicide, their thermoelectric properties and applications are discussed in Ref. 157.

14.3 $FeSi_2$ single crystals

Preparation of β-$FeSi_2$ single crystals has been carried out by chemical vapor transport (CVT) using I_2 as the transport agent and 5N purity starting materials.[154] In case of high purity materials, stoichiometric composition played an important role in determining transport properties. The thermoelectric properties of doped β-$FeSi_2$ single crystals grown using CVT comparison with polycrystalline β-$FeSi_{2+x}$ thin films prepared by e-beam evaporation and DC magnetron sputtering using source materials with different Si/Fe ratio were further studied in Ref. 158.

14.4 $FeSi_2$ polycrystalline/crystalline thin film

Iron disilicide thin films have been obtained by deposition techniques like electron beam evaporation (e.g., Ref. 159), magnetron sputtering (e.g., Ref. 160), RF sputtering (e.g., Ref. 162), and plasma ion processing (e.g., Ref. 161) followed by an annealing step. The results suggest that the thermoelectric properties vary widely depending upon the fabrication technology, purity of starting materials and the process conditions.

Effects of adding various p-type dopants like V, Cr, Mn and n-type dopants like Co, Ni, Pd, Pt were studied in Ref. 162. The films were deposited on Si discs by RF sputtering and then annealed to form crystalline doped $FeSi_2$. For the p-type dopants, V and Cr were found to yield better thermoelectric power factor than Mn (2.3×10^{-4} and $2.6 \times 10^{-4}\,W\,m^{-1}\,K^{-2}$ respectively at room temperature). For n-type dopants, Pt was the most suitable with power factor of $4.9 \times 10^{-4}\,W\,m^{-1}\,K^{-2}$.

14.5 $FeSi_2$: Powder metallurgical synthesis

The most conventional method of preparing bulk samples of β-$FeSi_2$ has been detailed in various publications (e.g., Ref. 163). The procedure involves smelting of the raw materials by induction or resistance heating. The ingot obtained is made into powder form by spraying or milling. This powder is densified by hot pressing or cold pressing and subsequent sintering. Annealing is then carried out to bring about phase transformation from metallic to semiconducting β-$FeSi_2$.

The most effective dopants for making n- and p-type $FeSi_2$ are Co and Mn/Al, respectively. The most efficient bulk

Table I. Summary of thermoelectric properties of $FeSi_2$ obtained by different dopants.

Type	Dopant	Type/Method	σ (S/cm)	S (μV/K)	PF ($W m^{-1} K^{-2}$)	κ ($W m^{-1} K^{-1}$)	Z_{max} (/K)	Temp. (K)	Ref.
	Co	Powder metallurgy	140–180	−200 to −220	—	7.5	3.43×10^{-4}	823	164, 171, 172
	Co	RF sputtering	53	−225	2.6×10^{-4}	—	—	300	162
	Co + Al	Powder metallurgy	260	−210	—	4.5	3.74×10^{-4}	823	163
	Co + Ge	Powder metallurgy	225	−160		5	1.26×10^{-4}	843	164
n-type	Co + Ru	Hot pressing	589	−160	1×10^{-3}	—	—	803	165
	Ni	RF sputtering	13	−113	1.7×10^{-5}	—	—	300	162
	Pd	RF sputtering	32	−241	1.9×10^{-4}	—	—	300	162
	Pt	RF sputtering	111	−202	4.9×10^{-4}	—	—	300	162
	Cu	Hot pressing	173	−173	8.53×10^{-4}	3.097	2.28×10^{-4}	933	37
	Cr	Powder metallurgy	40	370	—	7.5	5.2×10^{-5}	663	164
	Cr	RF sputtering	32	288	2.6×10^{-4}	—	—	300	162
	Cr + Ge	Powder metallurgy	90	240	—	6.7	6.6×10^{-5}	653	164
	Cr + Ru	Hot pressing	708	190	1.5×10^{-3}	4.6	3.35×10^{-4}	733	165
p-type	Mn	HP+annealing	50–150	200–380	—	—	—	150–900	171,172
	Mn	RF sputtering	4	81	2.4×10^{-6}	—	—	300	162
	Mn + Al	Mechanical alloying	—	270	—	5	1.3×10^{-4}	720	166
	V	RF sputtering	29	278	2.3×10^{-4}	—	—	300	162
	Zr	Mechanical alloying	3390	36	—	—	3.38×10^{-5}	1070	167

n-type β-$FeSi_2$ was found by partial compensation of Co with Al.[163] Effects of Cu and Ge doping in n- and p-type β-$FeSi_2$ were studied in Ref. 164. It was found that zT increases by the addition of Cr, Co, and Ge, but slightly decreases by addition of Cu. Efficient p-type β-$FeSi_2$ was also found by alloying with Ru and Cr.[165]

It was also shown in Refs. 166 and 167 that mechanical alloying can be used to produce homogeneous, fine-grained β-$FeSi_2$, without the need for heat treatment or any long-time annealing steps and can yield higher figure of merit due to smaller grain sizes.

In Refs. 168 and 169, bulk nanostructured β-$FeSi_2$ was prepared by melt spinning, rapid solidification and spark plasma sintering, which was found to significantly reduce the annealing time for phase transformation. Another fast method of preparation of Co and Mn-doped alloys by induction-field activated combustion/static pseudo isostatic compaction was studied in Ref. 170 and samples produced by this method were found to exhibit better thermoelectric properties than their hot-pressed and spark-plasma-sintered counterparts.

14.6 $FeSi_2$ thermoelectric properties

The literature consists of wide range of results that vary according to the method of fabrication, purity of the starting material, type of dopants and compositions, or annealing temperatures and time.[154] P-type material can be obtained from $FeSi_2$ by doping with transition elements lying on the left side of Fe in the periodic table, like Mn and Cr, while doping with elements on its right side, like Co and Ni yield n-type material. Approximate values of certain thermoelectric properties for different p- and n-type dopants are given in Table I. Also, Fig. 8 compares the thermoelectric properties of p-type iron disilicide with different dopants and compositions. Another noteworthy data was achieved for the nanocomposite of $(FeSi_2)_{0.75}(Si_{0.8}Ge_{0.2})_{0.25}$, which showed nearly 170% enhancement in zT compared to single phase β-$FeSi_2$[85] as shown in Fig. 9.

15. Cobalt monosilicide (CoSi)

Cobalt monosilicide is a semimetal, meaning that its band structure indicates a slight overlap of conduction and valence bands. It has a cubic crystal structure, a mass density of $6.58\,g/cm^3$, and melting temperature of 1450 °C. The room temperature Seebeck coefficient of $-83\,\mu V/K$, electrical conductivity of $1000\,S/cm$, and thermal conductivity of $20\,W\,m^{-1}\,K^{-1}$ has been reported by Ref. 173. It has been reported that strictly stoichiometric CoSi is n-type with carrier concentration of about $10^{20}\,cm^{-3}$.[174] Electron and hole effective masses are $2m_e$ and $6m_e$, respectively,[174] which means that the electron mobility is much higher than the hole mobility. The electron concentration can be increased by using Ni as the dopant or deceased by using Fe as a dopant. However, this substitution leads to a reduced Seebeck coefficient and figure-of-merit.[174]

Comparison of the thermoelectric properties of CoSi with various dopants is shown in Fig. 10. A study of thermal conductivities of CoSi shows that the lattice thermal conductivity makes up only a small fraction of the total thermal conductivity. Hence, nanostructuring and reduction of the grain sizes will not lead to an appreciable improvement in its thermoelectric efficiency. Alternative ways for improving the thermoelectric efficiency of CoSi has been suggested in Ref. 175, like reducing valence band and conduction band overlap by introducing crystal deformation or designing structures that strongly scatter only one type of carrier.

Many attempts have been made by different authors to improve the thermoelectric efficiency of CoSi. Doping of CoSi with Al has been studied in Refs. 173, 174, and 176, with Ge and B in Refs. 177, 178, and 179, and with Fe and Ni in Ref. 175. Moreover, effects of Ni, Pd, and Pt substitutions have been studied in Ref. 180. The comparison of the results obtained by these studies is shown in Fig. 10. Thermoelectric properties of $CoSi_{1-x}Al_x$ ($x = 0$ to 0.5) single crystals prepared by floating zone technique were studied in Ref. 174 and zT

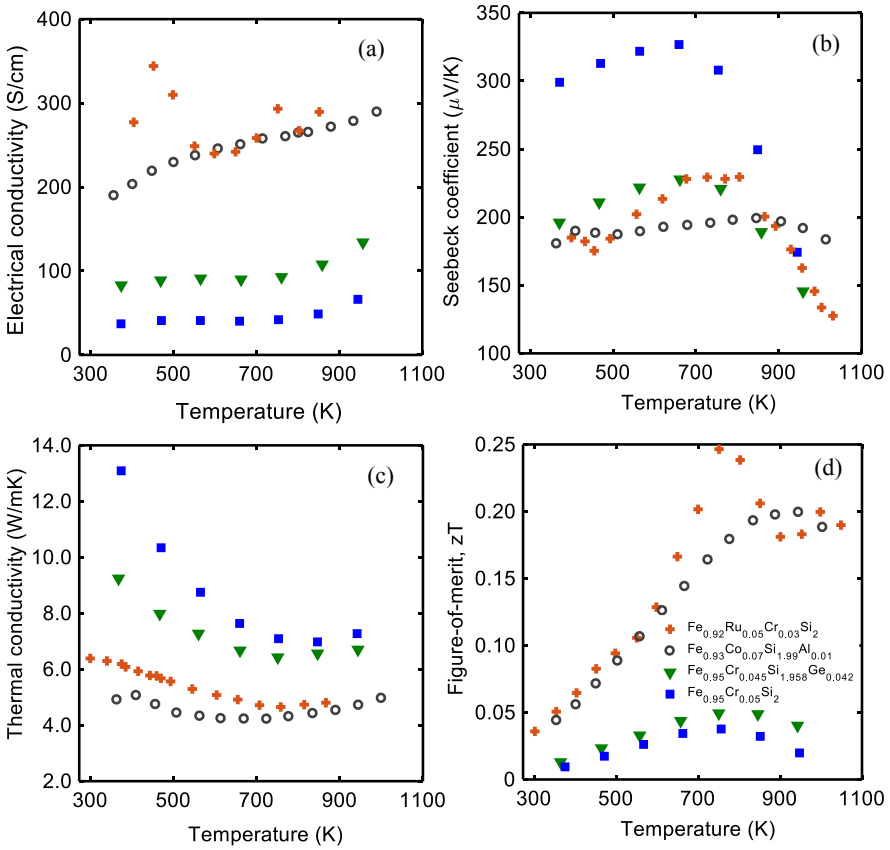

Fig. 8. (Color online) (a) Electrical conductivity, (b) Seebeck coefficient, (c) thermal conductivity, and (d) zT versus temperature for p-type $FeSi_2$ doped with (Cr, Cr+Ge, Ru) dopants. Refs: $Fe_{0.93}Co_{0.07}Si_{1.99}Al_{0.01}$,[163] $Fe_{0.95}Cr_{0.07}Si_{1.958}Ge_{0.042}$,[164] $Fe_{0.95}Cr_{0.05}Si_2$,[164] and $Fe_{0.92}Ru_{0.05}Cr_{0.03}Si_2$.[165] Figures created by author from the data in the mentioned sources.

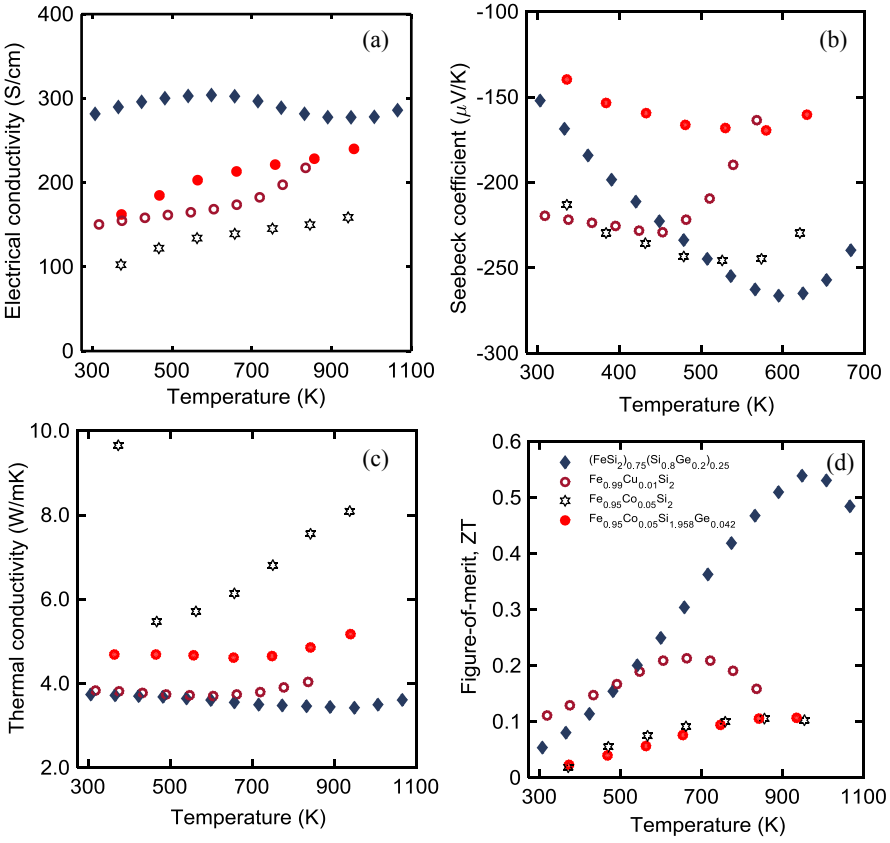

Fig. 9. (Color online) (a) Electrical conductivity, (b) Seebeck coefficient, (c) thermal conductivity, and (d) zT versus temperature for n-type $FeSi_2$ doped with Co,[37] Co+Ge,[164] and Cu[164] dopants, and nanocomposite of $(FeSi_2)_{0.75}(SiGe)_{0.25}$.[85] Figures created by author from the data in the mentioned sources.

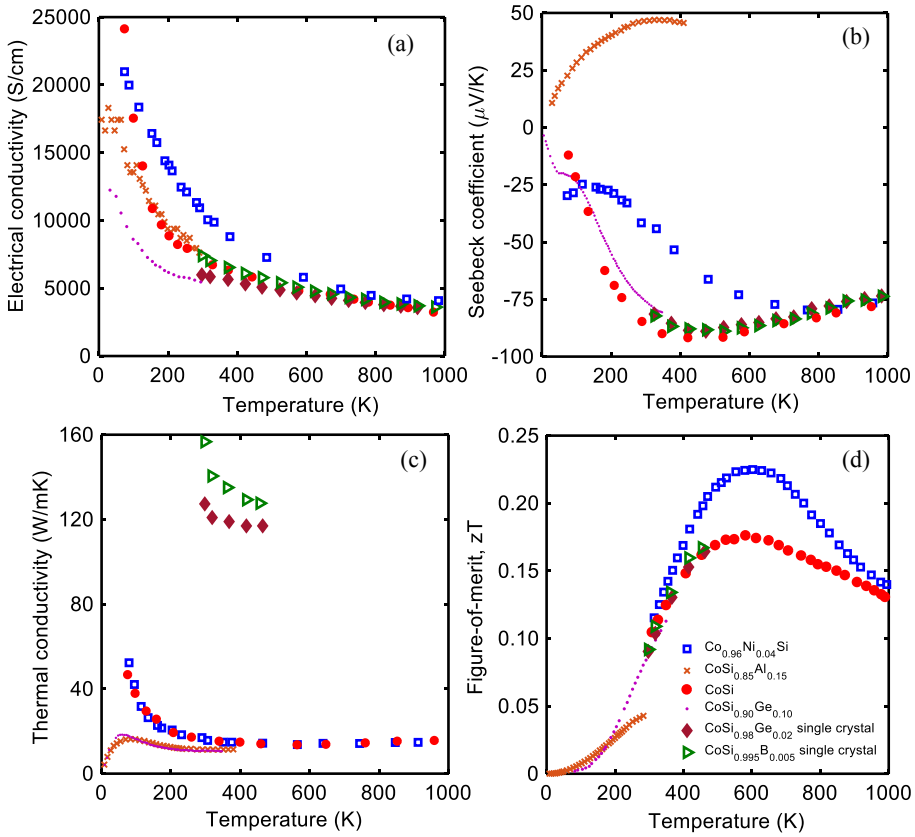

Fig. 10. (Color online) (a) Electrical conductivity, (b) Seebeck coefficient, (c) thermal conductivity, and (d) zT versus temperature for cobalt monosilicide obtained by various dopants. Refs: CoSi,[175] $Co_{0.96}Ni_{0.04}Si$,[175] $CoSi_{0.85}Al_{0.15}$,[173] $CoSi_{0.995}B_{0.005}$ single crystal,[177] $CoSi_{0.98}B_{0.02}$ single crystal,[177] and $CoSi_{0.90}Ge_{0.10}$.[179] Figures created by author from the data in the mentioned sources.

was found to be lower as compared to the undoped CoSi. Other studies have found that Al substitution dramatically decreases electrical resistivity and thermal conductivity. Although zT increased by increasing the amount of Al doping, it was still much lower than zT values of other thermoelectric materials.[173,176] Ge and B substitution, on the other hand, increased the thermoelectric power factor and figure of merit for single crystals[177,178] by reducing the electrical resistivity and thermal conductivity (see Fig. 10).

Thermoelectric performance of devices fabricated from $CrSi_2$–CoSi thermomodules was studied in Ref. 181. A comparison between materials made by high-purity versus low-purity starting material was made and it was found that 99% purity suffices for practical applications.

16. Cerium silicide ($CeSi_2$)

Pure $CeSi_2$ exhibits high electrical conductivity and low absolute value of the Seebeck coefficient ($\sigma \sim 106\,S/m$ and $S \sim -55\,\mu V/K$ at 300 K) in comparison with good thermoelectric materials.[182] $CeSi_2$ compounds are known to exhibit $GdSi_2$-type structure in low temperature, and $ThSi_2$ type structure in high temperature.[183] There are several $CeSi_2$ based compounds used as thermoelectric materials namely, $CeSi_2$, $Y_{0.5}Ce_{0.5}Si_2$, CeSiGa, CeSiGe, and $CeSi_{1.6}Ge_{0.4}$. These compounds can be fabricated by different methods like electric arc melting, milling, and thermal pressing. $CeSi_2$ and CeSiGa alloys exhibit metallic like conductivity with similar values of the electrical conductivity.[182–184] The electrical conductivity of CeSiGe and $Y_{0.5}Ce_{0.5}Si_2$ alloys are like semi-metallic materials, and $CeSi_{1.6}Ge_{0.4}$ shows semiconductors behavior.[183] It was found that the electrical conductivity of CeSiGe is strongly affected by Si(Ge) phase.[183] Seebeck coefficient, electrical conductivity, thermal conductivity and zT versus temperature of all mentioned materials are compared in Fig. 11.

17. Molybdenum silicide (Mo–Si) and tungsten silicide (W–Si)

Mo–Si based materials have multiple intermetallic compounds, namely, Mo_3Si, Mo_5Si_3, and $MoSi_2$. These materials have properties such as a high melting point, low electrical resistance, high-temperature stability and strength, and low density. They have usage as heating elements and protective coating.[185] Similarly, W_3Si, W_5Si_3, and WSi_2 phases exist in the W–Si based-materials. $MoSi_2$ and WSi_2 possess stable tetragonal phases and can be used as gate electrodes, interconnects and diffusion barriers in CMOS technology.[185,186] $MoSi_2$ and WSi_2 can be grown as epitaxial layers on Si substrates to form hexagonal phases. These two hexagonal materials have narrow bandgap.[186] The conventional fabrication method for Mo and W silicide is mechanical alloying.[184] Electrical conductivity and Seebeck coefficient of these two compounds are shown in Fig. 12. Mo- and W-silicide exhibit a narrow gap semiconductor behavior due to their temperature dependence of the conductivities. Also, both these silicides show p-type conductivity.[186]

Two different polymorphs of $MoSi_2$ are the α-$MoSi_2$, stable phase, and the β-$MoSi_2$, metastable phase.[185] α-$MoSi_2$

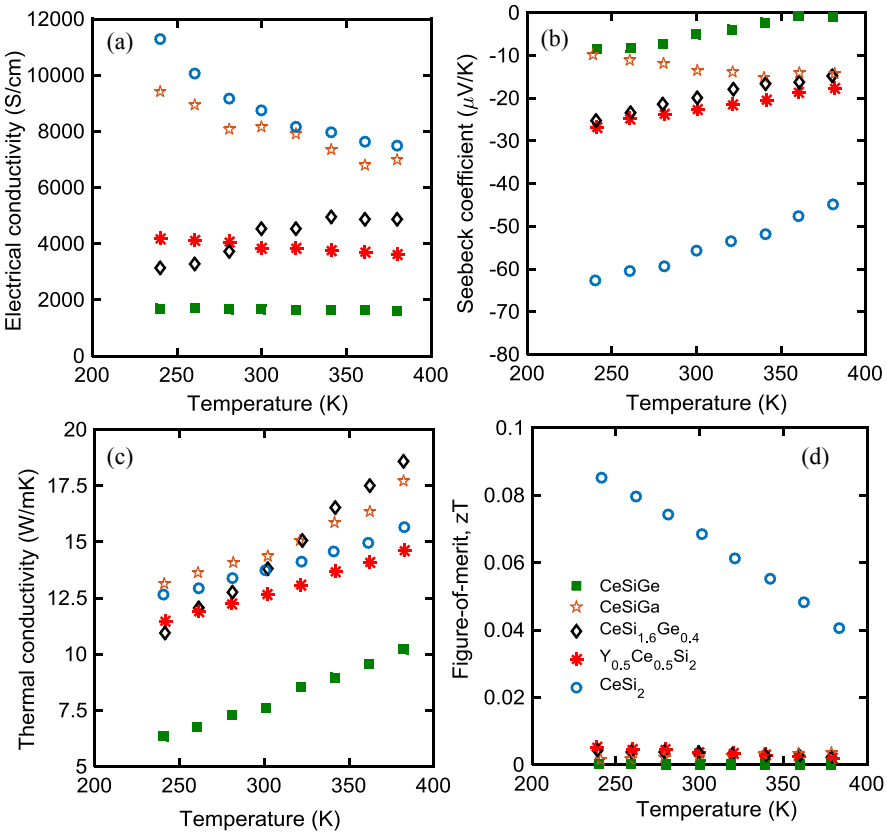

Fig. 11. (Color online) (a) Electrical conductivity, (b) Seebeck coefficient, (c) thermal conductivity, and (d) zT versus temperature for $CeSi_2$, $Y_{0.5}Ce_{0.5}Si_2$, CeSiGa, CeSiGe, and $CeSi_{1.6}Ge_{0.4}$ compiled from Ref. 183.

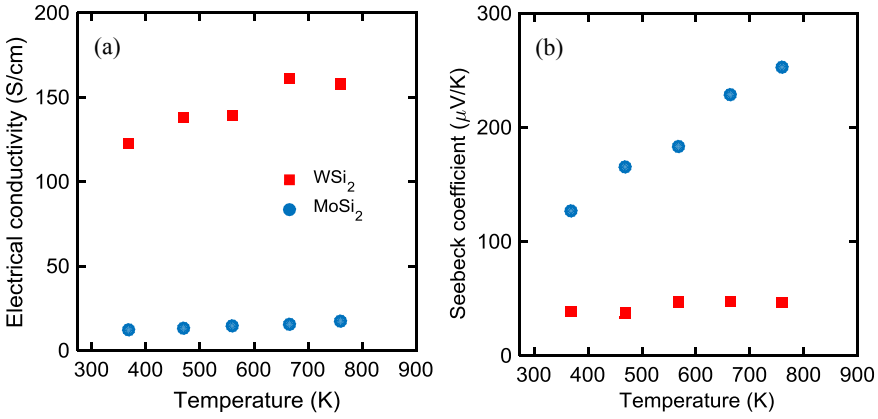

Fig. 12. (Color online) Comparison of (a) electrical conductivity and (b) Seebeck coefficient of $MoSi_2$ and WSi_2.[186)]

can be fabricated in amorphous, polycrystalline, and crystalline phase. β-$MoSi_2$ powders can be synthesized as amorphous phase by mechanical alloying or as a mixture with α-$MoSi_2$.[185)] Annealing β-$MoSi_2$ mixture in temperatures 973–1273 K can irreversibly transform it to α-$MoSi_2$.[185)] The crystal structure of α-$MoSi_2$ is the tetragonal body-centered $C11_b$ with space group $I4/mmm$ and the crystal structure of β-$MoSi_2$ is a hexagonal close-packed C40 with $P6_222$.[187)] Electrical conductivity and Seebeck coefficient versus temperature for α-$MoSi_2$ and β-$MoSi_2$ are shown in Fig. 13. It can be seen that both of these parameters increase with the temperature for both compounds; however, β-$MoSi_2$ has much higher Seebeck coefficient making it more suitable for thermoelectric applications.

It has been also showed that inclusion of $MoSi_2$ or WSi_2 nanoparticles in other silicides such as SiGe can decrease the thermal conductivity considerably resulting in a higher zT.[188,189)]

18. Lanthanum silicide (LaSi)

LaSi crystallizes with the orthorhombic FeB-type structure and the space group is *Pnma*. In comparison to other thermoelectric materials, for LaSi, both the electrical resistivity and Seebeck coefficient are very low (2.38 μΩ m and −1.5 μV/K at 333 K, respectively) and it behaves like metals. The Seebeck coefficient versus temperature for LaSi is shown in Fig. 14.[190)]

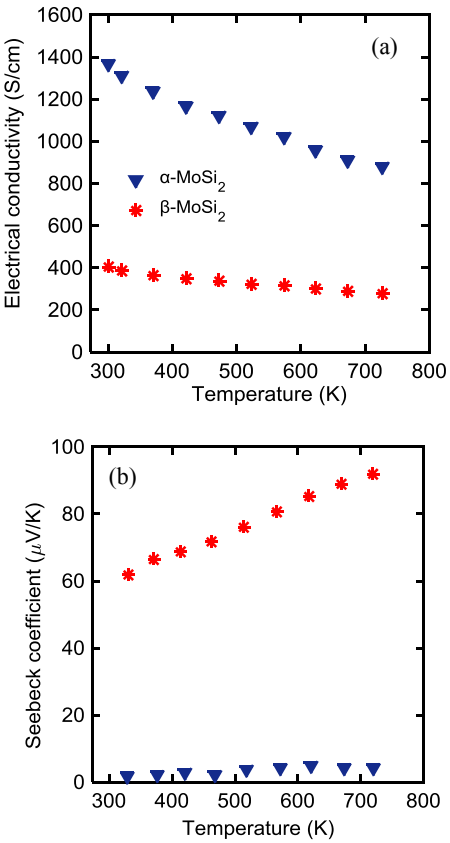

Fig. 13. (Color online) Comparison of (a) electrical conductivity and (b) Seebeck coefficient of α-$MoSi_2$ and β-$MoSi_2$.[185)]

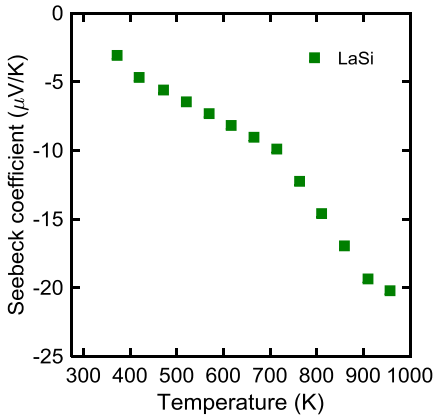

Fig. 14. (Color online) Seebeck coefficient of LaSi versus temperature.[190)]

19. Alkaline earth silicides

19.1 Strontium disilicide ($SrSi_2$)

Alkaline-earth-metal disilicide $SrSi_2$ is composed of non-toxic and naturally abundant elements which makes it an ecofriendly material. $SrSi_2$ is a narrow-gap semiconductor with a 35 meV band gap based on the electrical transport studies,[191)] whereas the band structure calculations predicted the presence of a sharp pseudogap of about 3 meV. However, a recent study estimated the value of band gap to be ~13 meV.[192)] $SrSi_2$ has a moderate Seebeck coefficient of about 130 μV/K at room temperature.[193)] Additionally, it possesses a fairly high electrical conductivity (~1000 S/cm).

Table II. The comparison of thermoelectric properties of $SrSi_2$-based alloys at room temperature.[193)]

Material	σ (S/cm)	S (μV/K)	κ ($W m^{-1} K^{-1}$)	zT
$Sr_{1.06}Si_2$	75	88.8	3.91	0.01
$SrSi_{1.94}Al_{0.06}$	602	63.1	5.23	0.01
$SrSi_2$	540	131.4	5.46	0.05
$Sr_{0.94}Si_2$	303	168.1	4.86	0.05
$Sr_{0.93}Ba_{0.07}Si_2$	704	156.7	4.90	0.11
$SrSi_{1.94}Ge_{0.06}$	775	144.3	5.10	0.13
$Sr_{0.9}Ca_{0.1}Si_2$	546	220.8	5.17	0.17
$Sr_{0.77}Ca_{0.1}Si_2$	719	143.9	1.66	0.27
$Sr_{0.92}Y_{0.08}Si_2$	3571	134.3	4.88	0.41

However, its high thermal conductivity (~5 $W m^{-1} K^{-1}$) hinders its thermoelectric performance.[194)] To improve its thermoelectric properties, a combination of three factors have been employed on the $SrSi_2$-based alloys:[192,195–197)] (a) lower electrical resistivity through the enhancement of the charge carriers, (b) higher Seebeck coefficient via the band structure engineering, and (c) lower thermal conductivity through the introduction of point defects or lattice imperfections. These improvements were made by introducing various dopants into the alloy to alter its properties. The effect of different dopants on the thermal and electrical properties is listed on Table II. In order to reveal the phonon–point-defect scattering effect on thermal conductivity of the $SrSi_2$-based alloys, lattice thermal conductivity of the pure, substituted and Sr-deficient/Sr-rich $SrSi_2$ alloys were evaluated. It was found that the Sr-deficient $Sr_{0.77}Ca_{0.1}Si_2$ alloy has the lowest room-temperature thermal conductivity value of about ~1.66 W $m^{-1} K^{-1}$ among the studied alloys shown in Table II.[193)] The table is ordered with respect to zT for comparison.

The estimated zT as a function of temperature for all optimized $SrSi_2$ alloys using the measured values of ρ, S, and κ is shown in Fig. 15. A reduction in zT value for the Al-substituted $SrSi_2$ was observed as a result of a considerable reduction in S value through hole doping (Kuo et al., 2012). On the other hand, the substitution of Ca, Ba, Y, and Ge elements in the $SrSi_2$ lead to an enhancement of their zT value over the entire temperature range of 10–300 K.[192,195,196)] A maximum room temperature zT value of about 0.41 has been attained for the $Sr_{0.92}Y_{0.08}Si_2$ alloy with a large thermoelectric power factor of 6.4×10^{-3} W $m^{-1} K^{-2}$ owing to the induced changes in the electronic band structure and carrier mobility through Y doping.[195)] The zT plot has a positive slope indicating that it will improve further at above room temperature. Moreover, for the so far most optimum alloy $Sr_{0.92}Y_{0.08}Si_2$, the lattice thermal conductivity is high (~4.88 W $m^{-1} K^{-1}$) indicating that a higher zT may be possible by nanostructuring to decrease the thermal conductivity.

Based on these results, it can be concluded that the $SrSi_2$ system is a potentially good candidate for thermoelectric applications if an optimal alloy is made. These encouraging findings suggest that the tuning of electronic band structure by suitable alloying/substitution along with right Sr-deficiency level could lead to enhancement of their thermoelectric performance.[198)]

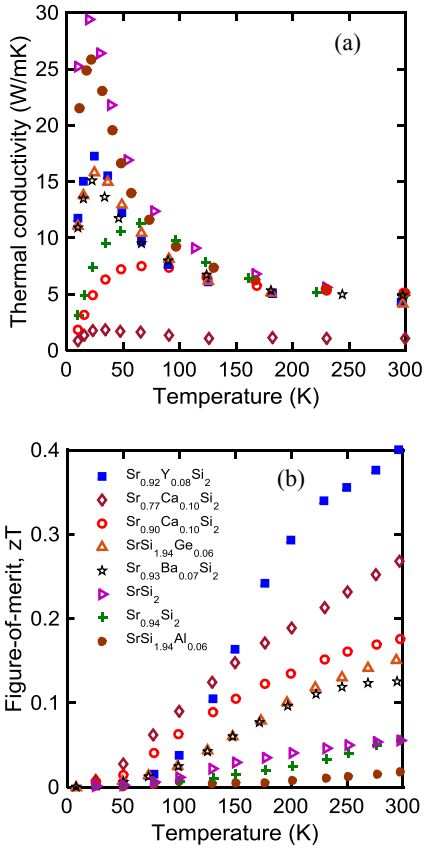

Fig. 15. (Color online) Comparison of (a) thermal conductivity and (b) zT of $SrSi_2$ obtained with various dopants.[193]

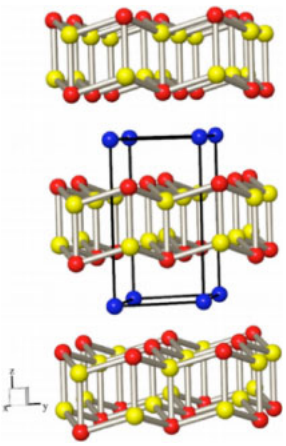

Fig. 16. (Color online) Crystal structure of $SrAl_2Si_2$. Red: Si, yellow: Al, blue: Sr.[199]

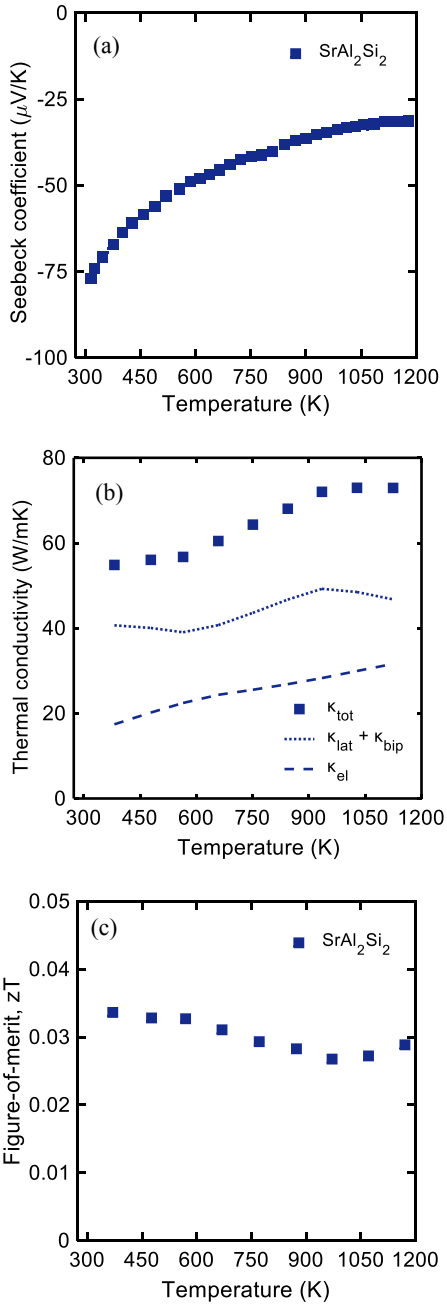

Fig. 17. (Color online) (a) Seebeck coefficient, (b) thermal conductivity, and (c) zT of $SrAl_2Si_2$ versus temperature.[199]

19.2 Strontium aluminum silicide ($SrAl_2Si_2$)

One of the more established alloys of $SrSi_2$ is with the addition of aluminum producing $SrAl_2Si_2$. The crystal structure of $SrAl_2Si_2$ is shown in Fig. 16.[199]

A high temperature metallic solution growth method was employed to prepare the single crystal of $SrAl_2Si_2$ from pure Si, Sr, and Al.[199] Its room temperature resistivity was 7–8 mΩ cm, which may be artificially high due to cracks in the crystals as the structure is fairly brittle. $SrAl_2Si_2$ is classified as a semimetal with the dominant carriers being holes below approximately 150 K and electrons above that temperature.[200] The transport is probably accounted for by both electrons and holes. The electrical resistivity decreases from 0.95 mΩ cm at room temperature to 0.6 mΩ cm at 1173 K with increasing temperature.[199] The isotropic mixture of crystallites could be the reason for its value being lower than that of a single crystal. Figure 17 shows the thermoelectric properties of $SrAl_2Si_2$. The Seebeck coefficient showed negative value from room temperature to 1173 K. The absolute value of the Seebeck coefficient decreased from 78 μV/K at room temperature to 34 μV/K at 1173 K with increasing temperature.[199] The resistivity and Seebeck coefficient values versus temperature are indicative of an intrinsic semiconductor. Minority p-type carriers are excited reducing the absolute Seebeck coefficient and resistivity with the increase of temperature. Thus, both n- and p-type carriers are operative in $SrAl_2Si_2$.

The figure of merit zT was calculated from the experimental electrical conductivity, Seebeck coefficient, and

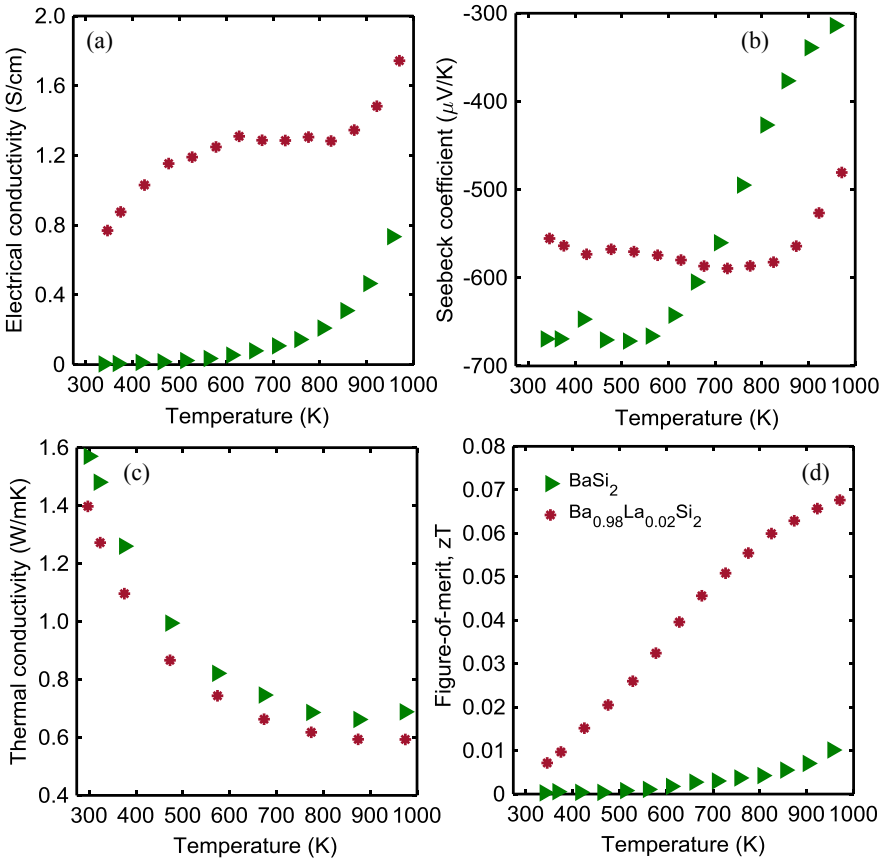

Fig. 18. (Color online) (a) Electrical conductivity, (b) Seebeck coefficient, (c) thermal conductivity, and (d) zT versus temperature of undoped crystalline $BaSi_2$ with La doped $Ba_{0.98}La_{0.02}Si_2$.[204)]

thermal conductivity. At the moment, the zT values being reported are not encouraging for thermoelectric applications, but established methods to lower thermal conductivity such as inducing structural disorder is a possibility. However, the presence of mixed (n- and p-type) carriers is the main reason that is limiting the zT. Therefore, it is necessary to increase the electronic band gap to eliminate the bipolar conduction.

19.3 Barium silicide ($BaSi_2$)

$BaSi_2$ is a semiconductor that crystallizes with the orthorhombic structure (space group: *Pnma*) at atmospheric pressure and room temperature. $BaSi_2$ has a large absorption coefficient and a band gap of 1.13 eV. This has been especially of interest for thin-film solar cell applications.[201)] Ba_2Si has been also considered for use as a thermoelectric material owing to its low thermal conductivity and high Seebeck coefficient. Temperature dependence of the electrical conductivity and Seebeck coefficient of undoped $BaSi_2$ are shown in Fig. 18. The data of these figures are from reference.[202,203)] The electrical conductivity of $BaSi_2$ increases with increasing temperature showing non-degenerate doped semiconductor behavior. The electrical conductivity values are approximately similar near room temperature,[202,203)] but they were slightly higher in Ref. 202 at high temperatures. $BaSi_2$ has a negative Seebeck value which is indicative of the majority charge carriers being electrons. The absolute S decreased with increasing temperature above approximately 550 K, which means that Ba_2Si entered the intrinsic region from this temperature. The thermal conductivity is small compared to most silicide thermoelectric materials indicating a good candidate for thermoelectric applications. The absolute S values were also relatively high, e.g., $-669\,\mu V/K$ at 337 K. However, the measured electrical conductivity was very low under 0.001–0.005 S/cm; hence, the power factor was very low less than $10^{-5}\,W\,m^{-1}\,K^{-2}$ over the whole temperature range. This low electrical conductivity is attributed to the low carrier density[204)] as the sample was undoped.

The thermoelectric properties of La doped $BaSi_2$ is also shown in Fig. 18. It can be seen that the electrical conductivity has improved significantly by 2% La doping. The Seebeck coefficient has reduced only moderately and the thermal conductivity has also reduced slightly. As a result, the zT has improved ~7 times compared to the undoped $BaSi_2$. The electrical conductivity of the doped $BaSi_2$ is still small and shows a low doped semiconductor trend versus temperature. Therefore, it is expected that with proper doping of $BaSi_2$ the power factor; hence the zT, should further improve.

19.4 Calcium silicide (CaSi, Ca_2Si, and Ca_5Si_3)

Calcium silicides has multiple phases that are stable at room temperature. Of those phases Ca_5Si_3 and Ca_2Si have been reported to show semiconducting behavior. It has been estimated by pseudopotential calculations that Ca_2Si has the energy gap of 0.36 eV.[10)] This makes the material attractive for thermoelectric applications. The thermoelectric properties of calcium silicide phases are shown in Fig. 19. The figure shows the thermoelectric properties of Ca_5Si_3 and CaSi. Ca_2Si was not measured because the material was too brittle to allow thermoelectric measurements.[205)] The measured electrical conductivity values for CaSi and Ca_5Si_3 are 4000

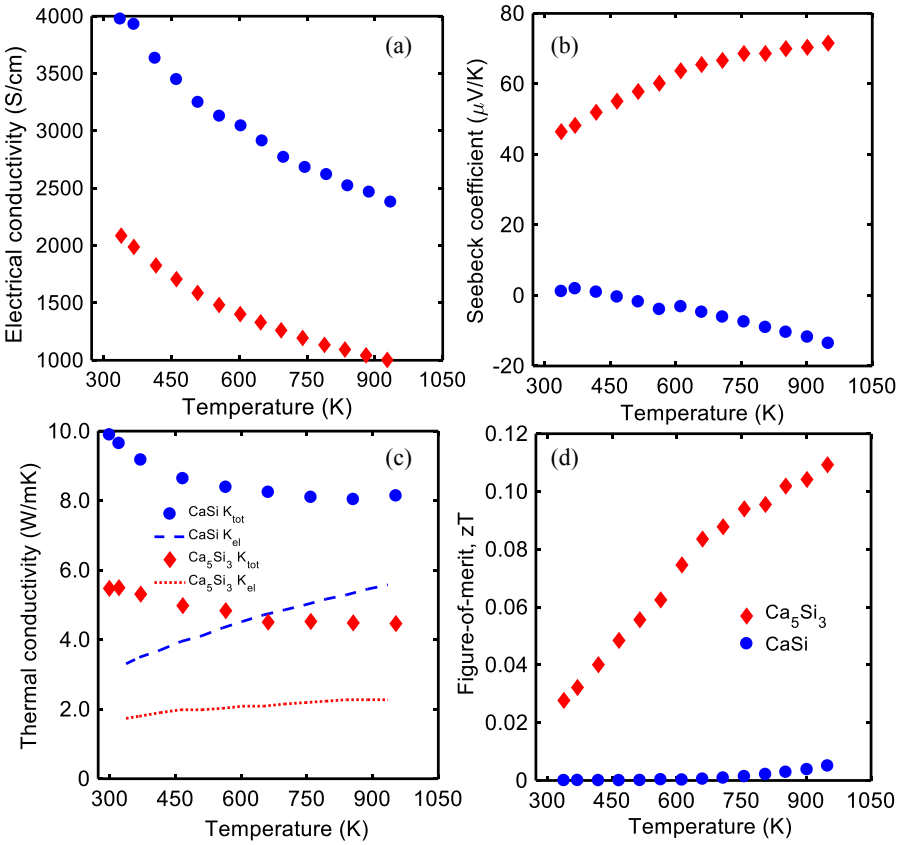

Fig. 19. (Color online) (a) Electrical conductivity, (b) Seebeck coefficient, (c) thermal conductivity, and (d) zT of CaSi and Ca_5Si_3 versus temperature.[205)]

and 2128 S/cm at 320 K, respectively. The electrical conductivity reduces with temperature indicating the metallic nature of the compounds. The magnitude of the Seebeck coefficient increases with increasing temperature for both samples. Both samples retain a positive Seebeck coefficient value until at about 320 K after which, in the case of CaSi, the Seebeck coefficient changes from positive to negative value with increasing temperature. This suggests that the majority carrier changes form hole to electron. Ca_5Si_3 shows positive Seebeck coefficient in all temperature ranges. The highest absolute value is observed for Ca_5Si_3 reaching 71 μV/K at 950 K.

In the thermal conductivity plot, the closed symbols show total thermal conductivity (κ_{total}) and the open symbols show the electronic thermal conductivity (κ_{el}). The ratios of the κ_{el} to the total thermal conductivity of both samples are about 50% at high temperature due to the large electrical conductivity. The lattice thermal conductivities of both samples decrease proportionally to T^{-1} indicating that phonon–phonon scattering is dominant in the temperature range. The lattice thermal conductivity of CaSi and Ca_5Si_3 reaches to 2.5 and 2.1 W/mK at about 970 K, respectively.[205)]

Table III lists some of the main properties of the silicide materials studied for thermoelectric applications so far. The values of thermal conductivity at temperature of highest zT and the peak zT values are also listed whenever available.

20. Thermoelectric module fabrication issues

While an overwhelming majority of thermoelectric research has been focused on developing and advancing material properties, it is equally important to address design challenges that ultimately sets the performance of a completed device. In general, there has been less effort in researching thermoelectric device issues in comparison to materials research, and this stands true for silicides as well. Two of the main challenges that face the integration of these materials into a device is in the metallization of contacts to the thermoelectric material, and the oxidation and sublimation that can become problematic at higher temperatures. A more detailed and in-depth look at these problems can be found in a review by Liu et al.[211)]

20.1 Metallization

A large challenge for interfacing thermoelectric materials with the metal interconnects between each leg is that they exhibit poor wettability to solders. In order to ensure good electrical bonding to the interconnects, thermoelectric materials must undergo a contact metallization which serves to increase its wettability and provide both a mechanically strong and low resistance bond. However, the metallization itself imposes a big challenge. The requirements for a good contact are (a) the metals must match the coefficient of thermal expansion (CTE) of the thermoelectric material to avoid mechanical failure at higher operating temperatures, (b) the metal contact must have low specific contact resistance with the thermoelectric material, and (c) the metal contact must exhibit good mechanical adhesion to the thermoelectric material.

20.2 Metal contacts to SiGe

Studies understanding the CTE and interface stresses of both nanostructured n and p-SiGe as well as mechanically alloyed (MA) SiGe where conducted by Ravi et al. at NASA's Jet Propulsion Laboratory (JPL).[212)] Their findings where that

Table III. Material properties of silicides.

Material	Type (n or p)	Lattice structure	Density (g/cm^3)	Melting point (°C)	Bandgap (eV)	κ at max. zT ($W\,m^{-1}\,K^{-1}$)	Max. zT	Temp. at max. zT (K)	Ref.[a)]
Mg_2Si	(n)	Cubic	1.99	1102	0.61–0.67	2.9	0.5–0.6	850	108, 107, 104
Mg_2Si	(p)	Cubic	1.96	1102	0.61–0.67	2.2	0.11	650	104, 111
$Mg_2(Si,Sn)$	(n)	Cubic	—	800	—	2.3	1.3	700	106
$Mg_2(Si,Sn)$	(p)	Cubic	—	800	—	2.5	0.5	750	109
Mg_2SiGe	(p)	Cubic	2.42	—	0.68	1.7	0.36	625	111
Mg_2SiGe	(n)	Cubic	1.97	—	—	2.4	0.74	756	108
$MnSi_x$	(p)	Tetragonal	5.186–5.23	1156.85	0.4–0.7	2.8–3.8	0.5–0.6	800	120, 82
$Si_{1-x}Ge_x$[b)]	(p)	Diamond	2.329–5.323	937–1412	0.66–1.12	2.39	0.95	1173	46, 44, 206
$Si_{1-x}Ge_x$[b)]	(n)	Diamond	2.329–5.323	937–1412	0.66–1.12	1.97–2.7	1.2–1.3	1073–1223	36, 37, 47
$ReSi_2$	(p)	Tetragonal	10.78	1977	0.12	—	—	—	—
$ReSi_{1.75}$	(p)	Triclinic		1940	0.16	4.6	0.7	1060	144
Ru_2Si_3	(n)	Orthorhombic	6.96	1697	0.8–1.1	2.2	0.2	900	146
URu_2Si_2	(p)	Tetragonal	—	~1800	0.1	~2.3	0.1	1082	147
USi_3	(p)	Cubic	—	~1600	—	~9	~0.3	1173	148
Os_2Si_3	(p)	Orthorhombic	11.15	—	2.3	—	—	—	—
Ir_3Si_5	(p)	Monoclinic	10.12	1400	1.2	—	~0.3	1100	151
$CrSi_2$	(p)	Hexagonal	4.98	1470	0.32–0.35	12.1	0.25	980	137, 139
α-$FeSi_2$	(p)	Tetragonal	4.99	1217	Metallic	—	—	—	—
β-$FeSi_2$	(p)	Orthorhombic	4.93	Stable <928	0.7–0.95	4.6	0.25	750	165
β-$FeSi_2$	(n)	Orthorhombic	4.93	Stable <928	0.7–0.95	3.4–3.6	0.5	890–1050	85
CoSi	(p)	Cubic	6.58	1450	−0.041	11	0.04	300	173
CoSi	(n)	Cubic	6.58	1450	−0.041	14	0.35	400	175
$CoSi_{1-x}Ge_x$	(n)	Cubic	6.58	1450	—	10.5	0.1	350	179
$SrAl_2Si_2$	(n), (p)	Hexagonal	2.924	1020	~0.02	~55	0.034	381	199
$BaSi_2$	(n)	Orthorhombic	3.54–3.68	1180	1.13–1.30	0.6	0.07	950	204
$SrSi_2$	(n)	Cubic	3.35	1100	0.013–0.035	~5.5	0.4	300	193, 207
CaSi	(n)	Orthorhombic	2.31	1324	—	2.5	5.1×10^{-3}	950	205
Ca_5Si_3	(p)	Tetragonal	—	—	—	2.1	0.11	950	205
$CaSi_2$		Cubic	2.5	1020	0.36	—	—	—	—
$MoSi_2$	(p)	Body-centered tetragonal	6.28	~2030	—	48.5	—	—	—
β-$MoSi_2$	(p)	Hexagonal	6.32	~1900	0.07	—	—	—	—
β-$MoSi_2$	(n)	Hexagonal	6.32	~1900	0.07	—	—	—	—
WSi_2	(p)	Hexagonal	9.88	~2160	0.07	—	—	—	—
$CeSi_2$	(n)	Tetragonal	5.31	1620	—	12.6	0.085	240	183
LaSi	(n)	Orthorhombic	—	1620	0.19	6.71	0.002	957	53, 194

a) The listed references are for the thermal conductivity and zT values. The references for some other material properties are Refs. 208, 209, and 210.
b) Density (g/cm^3): $2.329 + 3.493x - 0.499x^2$, Melting point (°C): $1412 - 738x + 263x^2$ (solidus) and $1412 - 80x - 395x^2$ (liquidus), Bandgap (eV): for $x < 0.85$: $1.12 - 0.41x + 0.008x^2$ for $x > 0.85$: $1.86 - 1.2x$.

under three cyclic temperature tests from 323 to 1273 K the coefficient of variation (CV) for the three materials where 0.05, 12.33, and 4.72% and CTE's of 4.6, 4.4, and 6.0×10^{-6}/K for p-type, n-type nanostructured SiGe, and MA-SiGe, respectively. Simulations concluded that these expansions promote permanent length changes which lead to stresses that could cause cracks and mechanical failure at the thermoelectric-metal contact interface. Proper matching of the CTE of the metal to the thermoelectric material is required in order to ensure reliable application. Many studies have been previously conducted for low resistivity SiGe contacts for source drain formation in CMOS transistors and have found $TiSi_2$ and $CoSi_2$ as suitable candidates.[213–215)] However, these materials do not meet the mechanical requirements of CTE when operated at higher temperatures. Mo and W are more promising candidates as their natural CTEs are around $\sim(4–5) \times 10^{-6}$/K, respectively.[211)] When alloyed with Cu whose CTE sits higher at around 16.5×10^{-6}/K, they can be tuned to have a range of CTE's depending on the alloy composition ratios. To this point, more in depth studies need to be performed on the reliability of these contacts.

20.3 Metal contacts to $MnSi_2$

Petrova et al. explored the diffusion of Cr and Cr/Ni contacts on HMS, $MnSi_{1.75}$ after 3 h of annealing at 1120 K.[216)] Their findings where that Cr diffuses into the HMS forming two distinct Cr–Mn–Si phases, $Cr_{3-q}Mn_pSi$ and $Mn_{1-p}Cr_pSi$. However, the Cr/Ni stack showed a reduction in Cr diffusion into Mn due to the diffusion of Ni itself into the Cr and Mn regions and allowed only one Cr–Mn–Si phase to form, notably the $Cr_{3-q}Mn_pSi$ phase. This reduction in Cr diffusion

from the Cr/Ni contact not only displayed the same high electrical and thermal conduction of the Cr contact, but showed improved mechanical properties as well since a higher concentration of Cr at the interface prevents interfacial pore formation. Further investigations studied Cu and Ni contacts directly sintered with the $MnSi_2$ material.[217,218] Electrical resistances were suitable for both but the authors noted the lack of mechanical stability under thermal stresses. Shi et al. further explored elemental Co, Ni, Cr, Ti, and Mo as well as MnSi and α-TiS_2 as contacts for HMS.[219] Their findings confirmed that while elemental contacts showed low electrical resistivity's, their CTE mismatch to the HMS was significant and caused poor mechanical bonding to the HMS and therefore is unreliable. On the other hand, silicide contacts, MnSi and α-TiS_2 showed greatly improved mechanical stability as the CTE closer matches that of HMS. Measurements of the contact resistance versus temperature showed comparable values between 10^{-4} to $10^{-5}\,\Omega\,cm^2$ for the contacts sintered directly on HMS. This study also showed the improved contact resistances from 10^{-5} to $10^{-6}\,\Omega\,cm^2$ for finer, nano-grained powders of MnSi and α-TiS_2.

20.4 Metal contacts to Mg_2Si

Nemoto et al. investigated an Al-doped n-type Mg_2Si device with Ni-contact (similar CTE to the thermoelectric material) metalized joined together with an Ag brazing to a Ni interconnect electrode.[220] The resistivity of the individual leg was measured to be $6.52 \times 10^{-6}\,\Omega\,cm^2$ leading to an ideal theoretical leg resistance of 3.86 mΩ. Actual measured resistance after all the contacts were added increased to 6.2 mΩ which lead to a contact resistance of $2 \times 10^{-3}\,\Omega\,cm^2$. Ideally the contact resistance should be at least an order of magnitude smaller than that of the thermoelectric material (typically $<10^{-5}\,\Omega\,cm^2$ for bulk thermoelectrics) as to not contribute additional parasitic resistance losses. The contact resistance, more notably the specific contact resistance between the contact metal and the thermoelectric leg is a problem of energy band alignments at the interface, i.e., choosing work functions of metals that minimize the energy barrier between the two and allow for low resistances. However, it has been known that having a high doping level at this interface can also help with resistances by allowing for not only thermionic emission of charge carriers over the Schottky barrier but tunneling through as well.[211] The authors in this study noted that this could be a useful technique for reducing the resistance between Ni and Mg_2Si. This improvement was investigated again by Nemoto et al. with Sb-doped Mg_2Si legs.[221] Similar to the last experiment, the study employed sintering Ni Contacts directly on the thermoelectric material. It was observed that the calculated specific contact resistance dropped to $7.8 \times 10^{-4}\,\Omega\,cm^2$ with the Sb doped samples and when the Cu electrodes replaced the Ni interconnects, a further reduction down to $5.9 \times 10^{-4}\,\Omega\,cm^2$. While a large improvement, this is still approximately an order of magnitude less than what is needed not to negatively impact the device performance; therefore, further studies on contacts to Mg_2Si material system is needed.

20.5 Sublimation and oxidation

Another consideration when integrating these materials into devices is how they react with the ambient at higher temperatures. Oxidation can lead to degradation in material quality and when operated at higher temperatures, sublimation or vaporization of the material into a gas can cause permanent physical changes to the thermoelectric leg that could lead to both electrical and mechanical issues. Careful investigation into the SiGe based RTG for NASA's Voyager 1 mission was conducted in order to assure the device endured a 50-year lifetime at high operating temperatures.[222] Without the coatings, the precipitation and eventual vaporization of Ge from the SiGe would occur at the outer surfaces of the material, changing both the mechanical and electrical properties. Chemical vapor deposited (CVD) SiO_2 and Si_3N_4 coatings around the legs were used as a means to suppress the sublimation control.[223] SiO_2 was found, however, to react with the silicon in the SiGe and create silicon monoxide, which is highly volatile. Therefore, Si_3N_4 and in combination with an argon gas was used as sufficient coating. Recently, in order to improve and slow down the sublimation rates even further, aerogels have been employed as a filler material in between the legs, instead of a vacuum or gas atmosphere.[223] Tests using skutterudite based materials who have similar sublimation rates to that of SiGe where conducted in order to evaluate the aerogels. The micro porous structure makes it exceedingly difficult for Ge diffusion out of the leg and the low thermal conductivity of the aerogel ensures little heat leakage both vertically and laterally between the hot/cold side contacts and between the legs, respectively. The tests showed a 700 fold improvement in sublimation rates between uncoated and coated samples. This process is believed to likely show the same improvements in other thermoelectric materials such as those in SiGe. There has been severe lack of studies investigating the longevity of other silicide thermoelectric materials at higher temperatures. While sublimation rates may not exhibit a large risk at operating temperature ranges of Mg_2Si and $MnSi_x$, long term oxidation issues could be an issue. Tani et al. studied the oxidation behavior of Mg_2Si and tested the improvement of oxidation resistance with a β-$FeSi_2$ coating at 873 K.[224] They found that oxygen diffuses into the Mg_2Si at temperatures above 723 K to yield volatile MgO and Si. Coatings of β-$FeSi_2$ showed to increase oxidation resistance by preventing the diffusion of oxygen into the silicide.

21. Future perspective of silicide thermoelectrics

Although the primary goal in thermoelectric community is achieving highest possible zT, other factors including the cost and device related issues, such as reliability, ease of fabrication, endurance, oxidation, etc., are equally important to be able to compete with other technologies. Hence, developing inexpensive, nontoxic and easily processed materials and competitive devices is equally important in research endeavors. Some silicide alloys have been identified so far that may meet such requirements, which has been the motivations for studying these materials.

A high peak zT does not necessarily produce an efficient device. At device level, a high zT over the working temperature and also across the hot to cold side temperature is important to achieve a high efficiency. According to Table III, silicide thermoelectrics have the potential to cover thermoelectric applications over a broad temperature range. While some silicides such as SiGe, Mg_2Si, $MnSi_{1.7}$, and $FeSi_2$ have been extensively studied and their thermoelectric properties have been optimized from various angels, some

other silicides such as $BaSi_2$, $SrSi_2$, CoSi, $ReSi_{1.75}$, and Ru_2Si_3 and have also shown promising band structure and lattice properties, which can make them good candidates for thermoelectric application. However, there have been relatively less efforts in optimizing their properties. As a first step, carrier concentration optimization by doping may produce much higher zT than what has been measured. In addition, other techniques such as nanostructuring and band engineering may be used to further improve the properties of these silicides.

To this end, a computationally guided material research can help to predict the important properties, i.e., electrical conductivity, Seebeck coefficient and thermal conductivity, and to find the optimum doping concentration. It is well known today that the ideal thermoelectric material is described as phonon-glass, electron-crystal and has ideally the low thermal conductivity of a glass but the high electrical conductivity of a crystal. However, even if the lattice thermal conductivity is small like a glass, a high electrical conductivity will result in a high electronic thermal conductivity that will still limit the zT. Therefore, it is highly desired to find ways to reduce the electronic thermal conductivity, or the relevant Lorentz number. In addition, reducing the acoustic phonon deformation potential can enhance the carrier mobility as well as the Seebeck coefficient in materials that phonon scattering is dominant, which applies to many good thermoelectric materials. Such requirements call for theoretical study of the electron and phonon transport and their interaction at fundamental levels. Atomistic modeling provides better insights to understand the transport properties so that the underlying physical mechanisms can be identified and exploited in the design of new generation of thermoelectric materials.

In recent years, researchers have explored bulk materials, with a focus on those with large unit-cells,[225] such as clathrates, which contain angstrom-sized internal cages.[226] The presence of rattle atoms inside these cages or through the small-scale disorder present at the unit cell level can prohibit phonon transport in these materials and decrease the lattice thermal conductivity significantly. The electrical conductivity is related to the material's Fermi energy. In an un-doped semiconductor, where the Fermi energy lies between the valence band and the conduction band, the electrons are bound to the atomic nuclei, and the electrical conductivity is very low while in doped semiconductors the electrical conductivity can approach to that of metals, which is a more appropriate choice for thermoelectric applications. The Seebeck coefficient and thermal conductivity are also related to the material's Fermi energy; therefore, the Fermi energy must be optimized considering all parameters to achieve an optimum zT. For solids at room temperature, the thermal conductivity may vary from about $0.01\,W\,m^{-1}\,K^{-1}$ for aerogels to a few thousand $W\,m^{-1}\,K^{-1}$ for carbon nanotubes and graphene. Amorphous materials have a room-temperature thermal conductivity of $\sim 0.5\,W\,m^{-1}\,K^{-1}$ and silicon, $\sim 150\,W\,m^{-1}\,K^{-1}$. Thermal conductivity has two major sources electrons (mostly in metals) and phonons (mostly in non-metals). Knowledge of a material's electronic band structure and the mobility of the electrons is necessary to predict electrical conductivity, the Seebeck coefficient and the electronic contribution to the thermal conductivity. As the behavior of electrons may be governed by the Schrödinger equation, and quantum based calculations are required at fundamental levels which often necessitates very powerful computational resources and limits the research progress.

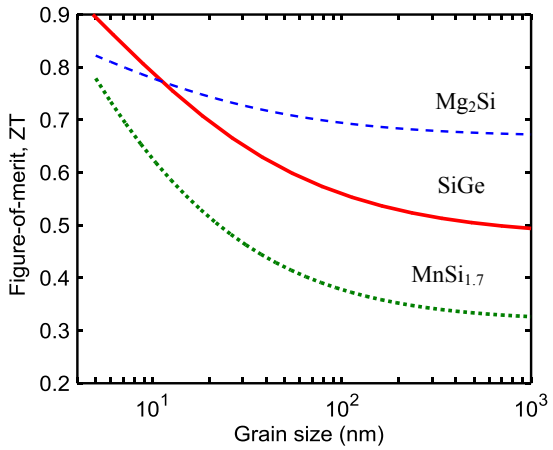

Fig. 20. (Color online) Predicted zT versus grain size for nanostructured p-type $Si_{0.8}Ge_{0.2}$, Mg_2Si, and $MnSi_{1.7}$.

21.1 Nanostructuring

Nanostructuring and band convergence have been adopted to enhance the efficiency of thermoelectric properties. Nanoscale effects have been known since 1990s that can enhance the thermoelectric properties by reducing the thermal conductivity and enhancing the thermoelectric power factor through modifications of the density of states. However, most enhancements so far have been through thermal conductivity reduction with less success on the improvement of the thermoelectric power factor.

The phonon mean free path is typically longer than the electron mean free path; hence, almost any sort of nanostructuring technique can increase phonon scattering (through interfaces or free surfaces) allowing for a decrease of thermal conductivity. A study on the effect of nanostructuring of $MnSi_{1.73}$ revealed that although nanostructuring reduces lattice thermal conductivity, the increased loss of electrical conductivity due to increased scattering at grain boundaries prohibits significant enhancement of the figure-of-merit for Ref. 82. Whenever, crystallite sizes lie between phonon MFPs and carrier MFPs, the reduction in thermal conductivity is coupled to reduction in electrical conductivity and the benefits of nanostructuring are decreased. Another study on the effect of Mg_2Si presented similar results.[83] It was shown that the nanostructuring in Mg_2Si would not be significantly beneficial to enhance figure-of-merit due to the detrimental effect of grain boundary scattering on carrier mobility. However, similar studies have shown that the nanostructuring is effective for $Si_{0.8}Ge_{0.2}$ where the thermal conductivity reduced to nearly 40% for an average crystallite size of 20 nm without noticeable deterioration in electrical conductivity. These trends are compared in Fig. 20.

21.2 Valleytronics of thermoelectric materials

The technique to control over the valley degree of freedom is known as valleytronics, which provides another material design tool for engineering both thermal and electrical transport properties. Valleytronics and engineering the charge carrier transport via multiple valleys has been widely used for designing good thermoelectric materials.[81,227–229] It has been

generally thought that a multi-valley band structure can improve the thermoelectric power factor. However, more recent studies have shown that the interplay among the valleytronics parameters such as the degeneracy of the band, intervalley transitions, effective mass, scattering exponent, and the Fermi energy may result in improvements or degradation of any or all of the main thermoelectric properties.[230,231] For example, it was demonstrated that tuning the composition in $PbTe_{1-x}Se_x$ alloys can direct the convergence of 12 valleys which in turn results in a remarkable enhancement in power factor and zT.[229] Moreover, it has been shown that the extraordinary thermoelectric performance of n-type $CoSb_3$ skutterudites at high temperatures is resulted from convergence of a secondary conduction band with the degeneracy value of 12 with the primary band.[232] In another study on $Mg_2Si_{1-x}Sn_x$ solid solutions, using both ab-initio calculations and measurements, it was shown that compositional variations can lead to cross over of two conduction bands, which increases the band degeneracy and in turn rises the density-of-states effective mass at $x \sim 0.7$. At this composition, zT reached 1.3 around 700 K due to the enhanced power factor.[109] Such a band convergence with high degeneracy value has been reported for Si clathrates as well.[233] Clathrates have intrinsically low value of thermal conductivity, which, in combination with high degeneracy value of conduction bands, can exceptionally enhance the thermoelectric efficiency.[234] It has been revealed that the group of type VIII Si, Ge, and Sn clathrates has potentially large power factors due to the existence of a large number of carrier pockets near their band edges. The band structure calculations have shown that Si-VIII clathrate has 26 carrier pockets near their valence band edge.[234–236] It was also shown that Si-VIII and its derivatives intercalated by alkali and alkaline-earth atoms have conduction band degeneracy of 19 and 18, respectively.[234,235] Interestingly, the exceptionally high multi-valley band structure of the so far hypothetical Si_{46}-VIII near the Fermi energy can results in a giant power factor. Such a large power factor along with their well-known low thermal conductivity can make this group of clathrates promising thermoelectric materials.

22. Summary

A review of compounds of silicon and transition metal silicides used for thermoelectric applications was presented. Silicides are interesting for thermoelectric application due to several distinct characteristics. In addition to high efficiency, many of them are inexpensive, resistive to oxidation and degradation, mechanically robust, and non-toxic. Many of these materials also have lower density than bismuth and chalcogenide based alloys owing to the small density of silicon. The mainstream research activities to enhance the thermoelectric efficiency of silicides (and many other thermoelectric materials) have been focused on reducing the lattice thermal conductivity through techniques such as alloying, nanostructuring or defect engineering. These efforts have resulted in approaching the lower limit of thermal conductivity where the lattice thermal conductivity becomes comparable to the electronic thermal conductivity. Therefore, the focus is shifting towards the enhancement of the thermoelectric power factor with a focus on increasing the Seebeck coefficient. Engineering of quantum confinement, resonant impurity states to distort the electronic band structure, increasing the number of carrier pockets (or large band multiplicity) near the band edges, or hot carrier filtering through energy barriers are considered as some of the main directions in this context. However, to date, there is no clear roadmap for achieving many of these aims. Theoretical tools and computational advancements can help in the efforts to discover or design new materials. Identification of the underlying parameters that correlate the electron and phonon interaction can also help in designing materials with high thermoelectric power. Some of these techniques have been successfully implemented in several silicides such as $Mg_2(Si,Sn)$ and nanostructured SiGe with many other silicides yet to be engineered. Several metal silicides have shown a large power factor, but have not been very good thermoelectric materials because of their large electronic thermal conductivity. Therefore, material engineering that can reduce the electronic thermal conductivity is also highly desired.

Acknowledgments

This study is partially based upon work supported by Air Force Office of Scientific Research (AFOSR) under contract number FA9550-12-1-0225 and the National Science Foundation (NSF) under grant numbers EEC-1160483, ECCS-1351533, and CMMI-1363485.

1) G. S. Nolas, G. A. Slack, D. T. Modeli, T. M. Tritt, and A. C. Ehrlich, J. Appl. Phys. **79**, 4002 (1996).
2) J. P. Fleurial, T. Caillat, and A. Borshchevsky, Proc. 13th Int. Conf. Thermoelectrics, 1994, p. 40.
3) B. C. Sales, D. Mandrus, and R. K. Williams, Science **272**, 1325 (1996).
4) S. Q. Bai, X. Y. Huang, L. D. Chen, W. Zhang, X. Y. Zhao, and Y. F. Zhou, Appl. Phys. A **100**, 1109 (2010).
5) A. Saramat, G. Svensson, A. E. C. Palmqvist, C. Stiewe, E. Mueller, D. Platzek, S. G. Williams, D. M. Rove, J. D. Bryan, and G. D. Stucky, J. Appl. Phys. **99**, 023708 (2006).
6) S. R. Brown, S. M. Kauzlarich, F. Gascoin, and G. J. Snyder, Chem. Mater. **18**, 1873 (2006).
7) S. H. Yang, T. J. Zhu, T. Sun, J. He, S. N. Zhang, and X. B. Zhao, Nanotechnology **19**, 245707 (2008).
8) K. F. Hsu, S. Loo, F. Guo, W. Chen, J. S. Dyck, C. Uher, T. Hogan, E. K. Polychroniadis, and M. G. Kanatzidis, Science **303**, 818 (2004).
9) J. P. Heremans, V. Jovovic, E. S. Toberer, A. Saramat, K. Kurosaki, A. Charoenphakdee, S. Yamanaka, and G. J. Snyder, Science **321**, 554 (2008).
10) L. Zhao, S. Lo, Y. Zhang, H. Sun, G. Tan, C. Uher, C. Wolverton, V. P. Dravid, and M. G. Kanatzidis, Nature **508**, 373 (2014).
11) L. D. Hicks and M. S. Dresselhaus, Phys. Rev. B **47**, 12727 (1993).
12) G. Chen, Phys. Rev. B **57**, 14958 (1998).
13) R. Venkatasubramanian, E. Siivola, T. Colpitts, and B. O'Quinn, Nature **413**, 597 (2001).
14) D. Vashaee, Y. Zhang, A. Shakouri, G. Zeng, and Y. Chiu, Phys. Rev. B **74**, 195315 (2006).
15) D. Vashaee and A. Shakouri, J. Appl. Phys. **95**, 1233 (2004).
16) G. Zeng, X. Fan, C. LaBounty, E. Croke, Y. Zhang, J. Christofferson, D. Vashaee, A. Shakouri, and J. E. Bowers, MRS Proc. **793**, S2 (2003).
17) T. C. Harman, P. J. Taylor, M. P. Walsh, and B. E. LaForge, Science **297**, 2229 (2002).
18) J. M. O. Zide, D. Vashaee, G. Zeng, J. E. Bowers, A. Shakouri, and A. C. Gossard, Phys. Rev. B **74**, 205335 (2006).
19) J. M. Zide, D. O. Klenov, S. Stemmer, A. C. Gossard, G. Zeng, J. E. Bowers, D. Vashaee, and A. Shakouri, Appl. Phys. Lett. **87**, 112102 (2005).
20) W. Kim, S. L. Singer, A. Majumdar, D. Vashaee, Z. Bian, A. Shakouri, G. Zeng, J. E. Bowers, J. M. O. Zide, and A. C. Gossard, Appl. Phys. Lett. **88**, 242107 (2006).

21) X. Fan, G. Zeng, E. Croke, C. LaBounty, D. Vashaee, A. Shakouri, and J. E. Bowers, Electron. Lett. **37**, 126 (2001).
22) B. Poudel, Q. Hao, Y. Ma, Y. Lan, A. Minnich, B. Yu, X. Yan, D. Wang, A. Muto, D. Vashaee, X. Chen, J. Liu, M. S. Dresselhaus, G. Chen, and Z. Ren, Science **320**, 634 (2008).
23) A. M. Dehkordi and D. Vashaee, Phys. Status Solidi A **209**, 2131 (2012).
24) N. Satyala, A. Tahmasbi Rad, Z. Zamanipour, P. Norouzzadeh, J. S. Krasinski, L. Tayebi, and D. Vashaee, J. Appl. Phys. **115**, 044304 (2014).
25) K. Biswas, J. He, I. D. Blum, C. Wu, T. P. Hogan, D. N. Seidman, V. P. Dravid, and M. G. Kanatzidis, Nature **489**, 414 (2012).
26) N. Satyala, P. Norouzzadeh, and D. Vashaee, in *Nanoscale Thermoelectrics*, ed. X. Wang and Z. M. Wang (Springer International Publishing, Cham, 2014) Lecture Notes in Nanoscale Science and Technology, Vol. 16, Chap. 4.
27) N. Hirayama, T. Iida, H. Funashima, S. Morioka, M. Sakamoto, K. Nishio, Y. Kogo, Y. Takanashi, and N. Hamada, Jpn. J. Appl. Phys. **54**, 07JC05 (2015).
28) S. Tada, Y. Isoda, H. Udono, H. Fujiu, S. Kumagai, and Y. Shinohara, J. Electron. Mater. **43**, 1580 (2014).
29) Q. Zhang, J. He, T. J. Zhu, S. N. Zhang, X. B. Zhao, and T. M. Tritt, Appl. Phys. Lett. **93**, 102109 (2008).
30) Y. Hayakawa, M. Arivanandhan, Y. Saito, T. Koyama, Y. Momose, H. Ikeda, A. Tanaka, C. Wen, Y. Kubota, T. Nakamura, S. Bhattacharya, D. K. Aswal, S. M. Babu, Y. Inatomi, and H. Tatsuoka, Thin Solid Films **519**, 8532 (2011).
31) H. Mo, J. Liu, and M. C. Öztürk, MRS Proc. **745**, N4 (2002).
32) J. Liu and M. C. Öztürk, IEEE Trans. Electron Devices **52**, 1535 (2005).
33) E. Alptekin, C. J. Kirkpatrick, V. Misra, and M. C. Öztürk, IEEE Trans. Electron Devices **56**, 1220 (2009).
34) A. J. Minnich, H. Lee, X. W. Wang, G. Joshi, M. S. Dresselhaus, Z. F. Ren, G. Chen, and D. Vashaee, Phys. Rev. B **80**, 155327 (2009).
35) C. B. Vining and C. E. Allevato, Proc. 27th Intersociety Energy Conversion Engineering Conf. (IECEC-92), 1992, Vol. 3, p. 489.
36) A. Nozariasbmarz, Z. Zamanipour, P. Norouzzadeh, J. S. Krasinski, and D. Vashaee, RSC Adv. **6**, 49643 (2016).
37) A. Nozariasbmarz, P. Roy, Z. Zamanipour, J. H. Dycus, M. J. Cabral, J. M. LeBeau, J. S. Krasinski, and D. Vashaee, APL Mater. **4**, 104814 (2016).
38) N. Mingo and D. Hauser, Nano Lett. **9**, 711 (2009).
39) E. N. Nikitin, Sov. Phys. Tech. Phys. **3**, 20 (1958).
40) E. N. Nikitin, Sov. Phys. Tech. Phys. **3**, 23 (1958).
41) M. I. Fedorov, J. Thermoelectr. **2**, 51 (2009).
42) C. B. Vining, J. Appl. Phys. **69**, 331 (1991).
43) D. M. Rowe, *Thermoelectrics Handbook: Macro to Nano* (CRC Press, Boca Raton, FL, 2005).
44) Z. Zamanipour, X. Shi, A. M. Dehkordi, J. S. Krasinski, and D. Vashaee, Phys. Status Solidi A **209**, 2049 (2012).
45) A. Nozariasbmarz, A. Tahmasbi Rad, Z. Zamanipour, J. S. Krasinski, L. Tayebi, and D. Vashaee, Scr. Mater. **69**, 549 (2013).
46) G. Joshi, H. Lee, Y. Lan, X. Wang, G. Zhu, D. Wang, R. W. Gould, D. C. Cuff, M. Y. Tang, M. S. Dresselhaus, G. Chen, and Z. F. Ren, Nano Lett. **8**, 4670 (2008).
47) X. W. Wang, H. Lee, Y. C. Lan, G. H. Zhu, G. Joshi, D. Z. Wang, J. Yang, A. J. Muto, M. Y. Tang, J. Klatsky, S. Song, M. S. Dresselhaus, G. Chen, and Z. F. Ren, Appl. Phys. Lett. **93**, 193121 (2008).
48) B. L. Liao, B. Qiu, J. W. Zhou, S. Huberman, K. Esfarjani, and G. Chen, Phys. Rev. Lett. **114**, 115901 (2015).
49) F. A. Trumbore, Bell Labs Tech. J. **39**, 205 (1960).
50) Z. Zamanipour, J. S. Krasinski, and D. Vashaee, J. Appl. Phys. **113**, 143715 (2013).
51) J. P. Dismukes, L. Ekstrom, E. F. Steigmeier, I. Kudman, and D. S. Beers, J. Appl. Phys. **35**, 2899 (1964).
52) C. B. Vining, Proc. 9th Int. Conf. Thermoelectrics, 1990, p. 249.
53) C. B. Vining, *CRC Handbook of Thermoelectrics* (CRC Press, Boca Raton, FL, 1995) p. 277.
54) R. Amatya and R. J. Ram, J. Electron. Mater. **41**, 1011 (2012).
55) R. W. Olesinski and G. J. Abbaschian, Bull. Alloy Phase Diagrams **7**, 170 (1986).
56) *Landolt–Börnstein: Group IV Physical Chemistry* (Springer, Heidelberg, 2002) Vol. 19B1, p. 296.
57) M. Zhang, J. G. Wen, M. Y. Efremov, E. A. Olson, Z. S. Zhang, L. Hu, L. P. de la Rama, R. Kummamuru, K. L. Kavanagh, Z. Ma, and L. H. Allen, J. Appl. Phys. **111**, 093516 (2012).
58) *Landolt–Börnstein: Group IV Physical Chemistry* (Springer, Heidelberg, 1998) Vol. 5J, p. 1.
59) *Landolt–Börnstein: Group IV Physical Chemistry* (Springer, Heidelberg, 1993) Vol. 5C, p. 1.
60) *Landolt–Börnstein: Group IV Physical Chemistry* (Springer, Heidelberg, 1997) Vol. 5G, p. 1.
61) M. I. Fedorov and G. N. Isachenko, Jpn. J. Appl. Phys. **54**, 07JA05 (2015).
62) R. K. Pisharody and L. P. Garvey, Proc. 13th Intersoc. Energy Conversion Engineering Conf., 1978, p. 1963.
63) D. M. Rowe, J. Phys. D **7**, 1843 (1974).
64) C. M. Bhandari and D. M. Rowe, Proc. 2nd Int. Conf. Thermoelectric Energy Conversion, 1978, p. 32.
65) D. M. Rowe, V. S. Shukla, and N. Savvides, Nature **290**, 765 (1981).
66) D. M. Rowe and V. S. Shukla, J. Appl. Phys. **52**, 7421 (1981).
67) C. B. Vining and J.-P. Fleurial, Proc. 10th Symp. Space Nuclear Power and Propulsion, 1993, p. 10.
68) F. J. DiSalvo, Science **285**, 703 (1999).
69) L. E. Bell, Science **321**, 1457 (2008).
70) J. R. Szczech, J. M. Higgins, and S. Jin, J. Mater. Chem. **21**, 4037 (2011).
71) X. Fan, G. Zeng, C. LaBounty, D. Vashaee, J. Christofferson, A. Shakouri, and J. E. Bowers, Proc. 20th Int. Conf. Thermoelectrics, 2001, p. 405.
72) D. M. Rowe, Appl. Energy **40**, 241 (1991).
73) J. W. Vandersande and J.-P. Fleurial, 15th Int. Conf. Thermoelectrics, 1996.
74) A. Majumdar, Science **303**, 777 (2004).
75) L. D. Zhao, G. Tan, S. Hao, J. He, Y. Pei, H. Chi, H. Wang, S. Gong, H. Xu, V. P. Dravid, C. Uher, G. J. Snyder, C. Wolverton, and M. G. Kanatzidis, Science **351**, 141 (2016).
76) J. LaGrandeur, D. Crane, S. Hung, B. Mazar, and A. Eder, 25th Int. Conf. Thermoelectrics, 2006.
77) D. M. Rowe, Int. J. Innovations Energy Syst. Power **1**, 13 (2006).
78) D. Kraemer, B. Poudel, H.-P. Feng, J. C. Caylor, B. Yu, X. Yan, Y. Ma, X. Wang, D. Wang, A. Muto, K. McEnaney, M. Chiesa, Z. Ren, and G. Chen, Nat. Mater. **10**, 532 (2011).
79) G. R. Schmidt, R. L. Wiley, and R. L. Richardson, AIP Conf. Proc. **746**, 429 (2005).
80) J. P. Fleurial, P. Gogna, G. Chen, M. S. Dresselhaus, H. Lee, M. Y. Tang, Z. F. Ren, D. Wang, S. Bux, D. King, R. Kaner, and R. Blair, 6th European Conf. Thermoelectrics, 2008, I-04-1.
81) M. S. Dresselhaus, G. Chen, M. Y. Tang, R. Yang, H. Lee, D. Wang, Z. Ren, J.-P. Fleurial, and P. Gogna, Adv. Mater. **19**, 1043 (2007).
82) P. Norouzzadeh, Z. Zamanipour, J. S. Krasinski, and D. Vashaee, J. Appl. Phys. **112**, 124308 (2012).
83) N. Satyala and D. Vashaee, Appl. Phys. Lett. **100**, 073107 (2012).
84) N. Satyala and D. Vashaee, J. Appl. Phys. **112**, 093716 (2012).
85) M. Mohebali, Y. Liu, L. Tayebi, J. S. Krasinski, and D. Vashaee, Renewable Energy **74**, 940 (2015).
86) M. I. Fedorov and V. K. Zaitsev, in *Modules, Systems, and Applications in Thermoelectrics*, ed. D. M. Rowe (CRC Press, Boca Raton, FL, 2012) Chap. 11.
87) Y. Lan, A. J. Minnich, G. Chen, and Z. Ren, Adv. Funct. Mater. **20**, 357 (2010).
88) D. J. Bergman and O. Levy, J. Appl. Phys. **70**, 6821 (1991).
89) D. J. Bergman and L. G. Fel, J. Appl. Phys. **85**, 8205 (1999).
90) J. H. Bahk, Z. Bian, M. Zebarjadi, P. Santhanam, R. Ram, and A. Shakouri, Appl. Phys. Lett. **99**, 072118 (2011).
91) Z. Zamanipour and D. Vashaee, J. Appl. Phys. **112**, 093714 (2012).
92) K. A. Borup, J. de Boor, H. Wang, F. Drymiotis, F. Gascoin, X. Shi, L. Chen, M. I. Fedorov, E. Muller, B. B. Iversena, and G. J. Snyder, Energy Environ. Sci. **8**, 423 (2015).
93) G. J. Snyder and T. S. Ursell, Phys. Rev. Lett. **91**, 148301 (2003).
94) D. M. Rowe, *CRC Handbook of Thermoelectrics* (CRC Press, Boca Raton, FL, 1995).
95) H. J. Goldsmid and A. W. Penn, Phys. Lett. A **27**, 523 (1968).
96) C. B. Vining, W. Laskow, J. O. Hanson, R. R. Van der Beck, and P. D. Gorsuch, J. Appl. Phys. **69**, 4333 (1991).
97) M. Abudakka, A. Nozariasbmarz, L. Tayebi, J. S. Krasisnki, and D. Vashaee, Energy Harvesting Syst. **2**, 47 (2015).
98) J. A. Martinez, P. P. Provencio, S. T. Picraux, J. P. Sullivan, and B. S. Swartzentruber, J. Appl. Phys. **110**, 074317 (2011).
99) E. K. Lee, L. Yin, Y. Lee, J. W. Lee, S. J. Lee, J. Lee, S. N. Cha, D. Whang, G. S. Hwang, K. Hippalgaonkar, A. Majumdar, C. Yu, B. L. Choi, J. M. Kim, and K. Kim, Nano Lett. **12**, 2918 (2012).
100) S. M. Lee, D. G. Cahill, and R. Venkatasubramanian, Appl. Phys. Lett. **70**, 2957 (1997).
101) A. Samarelli, L. Ferre Llin, S. Cecchi, J. Frigerio, T. Etzelstorfer, E. Müller, Y. Zhang, J. R. Watling, D. Chrastina, G. Isella, J. Stangl, J. P. Hague, J. M. R. Weaver, P. Dobson, and D. J. Paul, J. Appl. Phys. **113**, 233704 (2013).
102) Y. Lee, A. J. Pak, and G. S. Hwang, Phys. Chem. Chem. Phys. **18**, 19544 (2016).
103) P. Norouzzadeh, A. Nozariasbmarz, J. S. Krasinski, and D. Vashaee,

J. Appl. Phys. **117**, 214303 (2015).
104) H. Udono, H. Tajima, M. Uchikoshi, and M. Itakura, Jpn. J. Appl. Phys. **54**, 07JB06 (2015).
105) K. Arai, A. Sasaki, Y. Kimori, M. Iida, T. Nakamura, Y. Yamaguchi, K. Fujimoto, R. Tamura, T. Iida, and K. Nishio, Mater. Sci. Eng. B **195**, 45 (2015).
106) W. Liu, X. Tan, K. Yin, H. Liu, X. Tang, J. Shi, Q. Zhang, and C. Uher, Phys. Rev. Lett. **108**, 166601 (2012).
107) N. Satyala, J. S. Krasinski, and D. Vashaee, Acta Mater. **74**, 141 (2014).
108) H. Ihou-Mouko, C. Mercier, J. Tobola, G. Pont, and H. Scherrer, J. Alloys Compd. **509**, 6503 (2011).
109) Q. Zhang, L. Cheng, W. Liu, Y. Zheng, X. Su, H. Chi, H. Liu, Y. Yan, X. Tang, and C. Uher, Phys. Chem. Chem. Phys. **16**, 23576 (2014).
110) Y. Niwa, Y. Todaka, T. Masuda, T. Kawai, and M. Umemoto, Mater. Trans. **50**, 1725 (2009).
111) H. Q. Ye and S. Amelinckx, J. Solid State Chem. **61**, 8 (1986).
112) O. Schwomma, H. Nowotny, and A. Wittmann, Monatsh. Chem. **94**, 681 (1963) [in German].
113) O. Schwomma, A. Preisinger, H. Nowotny, and A. Wittmann, Monatsh. Chem. **95**, 1527 (1964) [in German].
114) G. Flieher, H. Vollenkle, and H. Nowotny, Monatsh. Chem. **98**, 2173 (1967) [in German].
115) H. W. Knott, M. H. Mueller, and L. Heaton, Acta Crystallogr. **23**, 549 (1967).
116) G. Zwilling and H. Nowotny, Monatsh. Chem. **104**, 668 (1973) [in German].
117) U. Gottlieb, A. Sulpice, B. Lambert-Andron, and O. Laborde, J. Alloys Compd. **361**, 13 (2003).
118) L. D. Ivanova, N. K. Abrikosov, E. I. Elagina, and V. D. Khvostikova, Izv. Akad. Nauk SSSR, Neorg. Mater. **5**, 1933 (1969) [in Russian].
119) M. Iioka, D. Ishada, S. Kojima, and H. Udono, Phys. Status Solidi C **10**, 1808 (2013).
120) Z. Zamanipour, X. Shi, M. Mozafari, J. S. Krasinski, L. Tayebi, and D. Vashaee, Ceram. Int. **39**, 2353 (2013).
121) D. Y. Nhi Truong, H. Kleinke, and F. Gascoin, Intermetallics **66**, 127 (2015).
122) A. J. Zhou, T. J. Zhu, X. B. Zhao, S. H. Yang, T. Dasgupta, C. Stiewe, R. Hassdorf, and E. Mueller, J. Electron. Mater. **39**, 2002 (2010).
123) W. Luo, H. Li, F. Fu, W. Hao, and X. Tang, J. Electron. Mater. **40**, 1233 (2011).
124) X. Chen, A. Weathers, D. Salta, L. Zhang, J. Zhou, J. B. Goodenough, and L. Shi, J. Appl. Phys. **114**, 173705 (2013).
125) T. Itoh and N. Ono, MRS Proc. **1490**, 127 (2012).
126) W. Luo, H. Li, Y. Yan, Z. Lin, X. Tang, Q. Zhang, and C. Uher, Intermetallics **19**, 404 (2011).
127) S. V. Faleev and F. Léonard, Phys. Rev. B **77**, 214304 (2008).
128) C. Fu, H. Xie, T. J. Zhu, J. Xie, and X. B. Zhao, J. Appl. Phys. **112**, 124915 (2012).
129) X. Chen, S. N. Girard, F. Meng, E. Lara-Curzio, S. Jin, J. B. Goodenough, J. Zhou, and L. Shi, Adv. Energy Mater. **4**, 1400452 (2014).
130) A. Yamamoto, S. Ghodke, H. Miyazaki, M. Inukai, Y. Nishino, M. Matsunami, and T. Takeuchi, Jpn. J. Appl. Phys. **55**, 020301 (2016).
131) S. Ghodke, N. Hiroishi, A. Yamamoto, H. Ikuta, M. Matsunami, and T. Takeuchi, J. Electron. Mater. **45**, 5279 (2016).
132) X. She, X. Su, H. Du, T. Liang, G. Zheng, Y. Yan, R. Akram, C. Uher, and X. Tang, J. Mater. Chem. C **3**, 12116 (2015).
133) V. Ponnambalam, D. T. Morelli, S. Bhattacharya, and T. M. Tritt, J. Alloys Compd. **580**, 598 (2013).
134) D. Y. Nhi Truong, D. Berthebaud, F. Gascoin, and H. Kleinke, J. Electron. Mater. **44**, 3603 (2015).
135) M. Saleemi, A. Famengo, S. Fiameni, S. Boldrini, S. Battiston, M. Johnsson, M. Muhammed, and M. S. Toprak, J. Alloys Compd. **619**, 31 (2015).
136) S. Perumal, S. Gorsse, U. Ail, M. Prakasam, B. Chevalier, and A. M. Umarji, J. Mater. Sci. **48**, 6018 (2013).
137) I. Nishida, J. Mater. Sci. **7**, 1119 (1972).
138) M. C. Bost and J. E. Mahan, J. Appl. Phys. **63**, 839 (1988).
139) B. K. Voronov, L. D. Dudkin, and N. N. Trusova, *Khimicheskaya Svyaz v Poluprovodnikah* (Nauka i Tekhnika, Minsk, 1969) p. 291 [in Russian].
140) Z. J. Pan, L. T. Zhang, and J. S. Wu, Scr. Mater. **56**, 257 (2007).
141) Y. Ohishi, A. Mohamad, Y. Miyazaki, H. Muta, K. Kurosaki, and S. Yamanaka, J. Phys. Chem. Solids **87**, 153 (2015).
142) H. Nagai, T. Takamatsu, Y. Iijima, K. Hayashi, and Y. Miyazaki, J. Alloys Compd. **687**, 37 (2016).
143) U. Gottlieb, B. Lambert-Andron, F. Nava, M. Affronte, O. Laborde, A. Rouault, and R. Madar, J. Appl. Phys. **78**, 3902 (1995).
144) H. Inui, MRS Proc. **886**, 0886-F06-08 (2005).
145) D. J. Poutcharovsky, K. Yvon, and E. Parthe, J. Less-Common Met. **40**, 139 (1975).
146) B. A. Simkin, Y. Hayashi, and H. Inui, Intermetallics **13**, 1225 (2005).
147) Y. Arita, K. Terao, S. Mitsuda, Y. Nishi, T. Matsui, and T. Nagasaki, J. Nucl. Mater. **294**, 206 (2001).
148) L. H. Brixner, J. Inorg. Nucl. Chem. **25**, 783 (1963).
149) J. Schumann, D. Elefant, C. Gladun, A. Heinrich, W. Pitschke, H. Lange, W. Henrion, and R. Grotzschel, Phys. Status Solidi A **145**, 429 (1994).
150) C. E. Allevato and C. B. Vining, Proc. 28th Intersoc. Energy Conversion Engineering Conf. (IECEC-93), 1993, Vol. 1, p. 239.
151) W. Pitschke, R. Kurt, A. Heinrich, J. Schumann, H. Grießmann, H. Vinzelberg, and A. T. Burkov, J. Mater. Res. **15**, 772 (2000).
152) H. Udono, I. Kikuma, T. Okuno, Y. Masumoto, H. Tajima, and S. Komuro, Thin Solid Films **461**, 182 (2004).
153) M. C. Bost and J. E. Mahan, J. Vac. Sci. Technol. B **4**, 1336 (1986).
154) G. Behr, J. Werner, G. Weise, A. Heinrich, A. Burkov, and C. Gladun, Phys. Status Solidi A **160**, 549 (1997).
155) I. Yamauchi, S. Ueyama, and I. Ohnaka, Mater. Sci. Eng. A **208**, 108 (1996).
156) R. M. Ware and D. J. McNeill, Proc. IEE **111**, 178 (1964).
157) Y. Isoda and H. Udono, in *Materials, Preparation, and Characterization in Thermoelectrics*, ed. D. M. Rowe (CRC Press, Boca Raton, FL, 2012) Chap. 18.
158) A. Heinrich, H. Griessmann, G. Behr, K. Ivanenko, J. Schumann, and H. Vinzelberg, Thin Solid Films **381**, 287 (2001).
159) H. P. Geserich, S. K. Sharma, and W. A. Theiner, Philos. Mag. **27**, 1001 (1973).
160) M. Nikolaeva, M. Sendova-Vassileva, D. Dimova-Malinovska, D. Karpuzov, J. C. Pivin, and G. Beshkov, Vacuum **69**, 221 (2002).
161) K. Matsubara, N. Minemura, J. Miyata, K. Kishimoto, K. Kawamura, T. Koyanagi, and T. Miki, Proc. 10th Int. Conf. Therrnoelectrics, 1991, p. 40.
162) M. Komabayashi, K. Hijikata, and S. Ido, Jpn. J. Appl. Phys. **30**, 331 (1991).
163) E. Groβ, M. Riffel, and U. Stöhrer, J. Mater. Res. **10**, 34 (1995).
164) S. W. Kim, M. K. Cho, Y. Mishima, and D. C. Choi, Intermetallics **11**, 399 (2003).
165) H. Takizawa, P. F. Mo, T. Endo, and M. Shimada, J. Mater. Sci. **30**, 4199 (1995).
166) M. Umemoto, Mater. Trans. JIM **36**, 373 (1995).
167) M. Ito, H. Nagai, T. Tahata, S. Katsuyama, and K. Majima, J. Appl. Phys. **92**, 3217 (2002).
168) L. Han, X.-F. Tang, W.-Q. Cao, and Q.-J. Zhang, Chin. Phys. B **18**, 287 (2009).
169) X. Qu, S. Lü, J. Hu, and Q. Meng, J. Alloys Compd. **509**, 10217 (2011).
170) M. Shibuya, M. Kawata, Y. Shinohara, and M. Ohyanagi, Trans. Mater. Res. Soc. Jpn. **40**, 219 (2015).
171) I. Nishida, Phys. Rev. B **7**, 2710 (1973).
172) T. Kojima, Phys. Status Solidi A **111**, 233 (1989).
173) C. S. Lue, Y. K. Kuo, C. L. Huang, and W. J. Lai, Phys. Rev. B **69**, 125111 (2004).
174) C. C. Li, W. L. Ren, L. T. Zhang, K. Ito, and J. S. Wu, J. Appl. Phys. **98**, 063706 (2005).
175) M. I. Fedorov and V. K. Zaitsev, in *CRC Handbook of Thermoelectrics*, ed. D. M. Rowe (CRC Press, Boca Raton, FL, 1995) p. 299.
176) Z. J. Pan, L. T. Zhang, and J. S. Wu, Comput. Mater. Sci. **39**, 752 (2007).
177) W. L. Ren, C. C. Li, L. T. Zhang, K. Ito, and J. S. Wu, J. Alloys Compd. **392**, 50 (2005).
178) E. Skoug, C. Zhou, Y. Pei, and D. T. Morelli, Appl. Phys. Lett. **94**, 022115 (2009).
179) Y. K. Kuo, K. M. Sivakumar, S. J. Huang, and C. S. Lue, J. Appl. Phys. **98**, 123510 (2005).
180) H. Sun, X. Lu, and D. T. Morelli, J. Electron. Mater. **42**, 1352 (2013).
181) T. Tokushima, I. Nishida, K. Sakata, and T. Sakata, J. Mater. Sci. **4**, 978 (1969).
182) A. J. Zhou, T. J. Zhu, H. L. Ni, Q. Zhang, and X. B. Zhao, J. Alloys Compd. **455**, 255 (2008).
183) A. V. Morozkin, V. A. Stupnikov, V. N. Nikiforov, N. Imaoka, and I. Morimoto, J. Alloys Compd. **415**, 12 (2006).
184) V. N. Nikiforov, V. Y. Irkhin, and A. V. Morozkin, in *Low-Dimensional Functional Materials*, ed. R. Egger, D. Matrasulov, and K. Rakhimov (Springer, Dordrecht, 2013) NATO Science for Peace and Security Series B: Physics and Biophysics, Chap. 19.
185) T. Yamada and Y. Hisanori, Intermetallics **19**, 908 (2011).
186) T. Nonomura, C. Wen, A. Kato, K. Isobe, Y. Kubota, T. Nakamura, M. Yamashita, Y. Hayakawa, and H. Tatsuoka, Phys. Procedia **11**, 110 (2011).
187) F. M. d'Heurle, C. S. Petersson, and M. Y. Tsai, J. Appl. Phys. **51**, 5976

(1980).
188) K. Favier, G. Bernard-Granger, C. Navone, M. Soulier, M. Boidot, J. Leforestier, J. Simon, J.-C. Tedenac, and D. Ravot, Acta Mater. **64**, 429 (2014).
189) J. Mackey, F. Dynsys, and A. Sehirlioglu, Acta Mater. **98**, 263 (2015).
190) K. Hashimoto, K. Kurosaki, Y. Imamura, H. Muta, and S. Yamanaka, 26th Int. Conf. Thermoelectrics (ICT 2007), 2007, p. 245.
191) Y. Imai and A. Watanabe, Intermetallics **14**, 666 (2006).
192) C. S. Lue, C. N. Kuo, J. Y. Huang, H. L. Hsieh, H. Y. Liao, B. Ramachandran, and Y. K. Kuo, J. Phys. D **46**, 315303 (2013).
193) Y. K. Kuo, B. Ramachandran, and C. S. Lue, Front Chem. **2**, 1 (2014).
194) K. Hashimoto, K. Kurosaki, Y. Imamura, H. Muta, and S. Yamanaka, J. Appl. Phys. **102**, 063703 (2007).
195) C. S. Lue, M. D. Chou, N. Kaurav, Y. T. Chung, and Y. K. Kuo, Appl. Phys. Lett. **94**, 192105 (2009).
196) C. S. Lue, S. F. Wong, J. Y. Huang, H. L. Hsieh, H. Y. Liao, B. Ramachandran, and Y. K. Kuo, J. Appl. Phys. **113**, 013710 (2013).
197) Y. K. Kuo, C. S. Lue, G. Hsu, J. Y. Huang, and H. L. Hsieh, Mater. Chem. Phys. **137**, 604 (2012).
198) M. Imai, A. Sato, T. Kimura, and T. Aoyagi, Thin Solid Films **519**, 8496 (2011).
199) S. M. Kauzlarich, C. L. Condron, J. K. Wassei, T. Ikeda, and G. J. Snyder, J. Solid State Chem. **182**, 240 (2009).
200) M. Imai, H. Abe, and K. Yamada, Inorg. Chem. **43**, 5186 (2004).
201) T. Suemasu, T. Saito, K. Toh, A. Okada, and M. A. Khan, Thin Solid Films **519**, 8501 (2011).
202) M. Imai and T. Hirano, J. Alloys Compd. **224**, 111 (1995).
203) T. Nakamura, T. Suemasu, K. Takakura, F. Hasegawa, A. Wakahara, and M. Imai, Appl. Phys. Lett. **81**, 1032 (2002).
204) K. Hashimoto, K. Kurosaki, H. Muta, and S. Yamanaka, Mater. Trans. **49**, 1737 (2008).
205) Y. Imamura, H. Muta, K. Kurosaki, and S. Yamanaka, Int. Conf. Thermoelectrics, 2006.
206) Z. Zamanipour, E. Salahinejad, P. Norouzzadeh, J. S. Krasinski, L. Tayebi, and D. Vashaee, J. Appl. Phys. **114**, 023705 (2013).
207) *CRC Handbook of Chemistry and Physics* (CRC Press, Boca Raton, FL, 2010) 90th ed.
208) R. C. Ropp, *Encyclopedia of the Alkaline Earth Compounds* (Elsevier, Amsterdam, 2013).
209) V. Borisenko, *Semiconducting Silicides: Basics, Formation, Properties* (Springer, Heidelberg, 2000) Springer Series in Materials Science, Vol. 39.
210) Landolt–Börnstein Online Library, Vol. III [http://www.springermaterials.com/].
211) W. Liu, Q. Jie, H. S. Kim, and Z. Ren, Acta Mater. **87**, 357 (2015).
212) V. Ravi, S. Firdosy, T. Caillat, E. Brandon, K. Van Der Walde, L. Maricic, and A. Sayir, J. Electron. Mater. **38**, 1433 (2009).
213) W. J. Qi, B. Z. Li, W. N. Huang, Z. G. Gu, H. Q. Lu, X. J. Zhang, M. Zhang, G. S. Dong, D. C. Miller, and R. G. Aitken, J. Appl. Phys. **77**, 1086 (1995).
214) W. J. Qi, B. Z. Li, G. B. Jiang, W. N. Huang, and Z. G. Gu, IEEE Region 10 Int. Conf. Microelectronics and VLSI (TENCON 95), 1995, p. 278.
215) M. Glück, A. Schüppen, M. Rösler, W. Heinrich, J. Hersener, U. König, O. Yam, C. Cytermann, and M. Eizenberg, Thin Solid Films **270**, 549 (1995).
216) L. I. Petrova, L. D. Dudkin, M. I. Fedorov, F. Y. Solomkin, V. K. Zaitsev, and I. S. Eremin, Inorg. Mater. **40**, 558 (2004).
217) Y. Thimont, Q. Lognoné, C. Goupil, F. Gascoin, and E. Guilmeau, J. Electron. Mater. **43**, 2023 (2014).
218) H. Fateh, C. A. Baker, M. J. Hall, and L. Shi, Appl. Energy **129**, 373 (2014).
219) X. Shi, Z. Zamanipour, J. S. Krasinski, A. Tree, and D. Vashaee, J. Electron. Mater. **41**, 2331 (2012).
220) T. Nemoto, T. Iida, J. Sato, T. Sakamoto, T. Nakajima, and Y. Takanashi, J. Electron. Mater. **41**, 1312 (2012).
221) T. Nemoto, T. Iida, J. Sato, T. Sakamoto, N. Hirayama, T. Nakajima, and Y. Takanashi, J. Electron. Mater. **42**, 2192 (2013).
222) F. de Winter, G. Stapfer, and E. Medina, IEEE Aerosp. Electron. Syst. Mag. **15**, 5 (2000).
223) J. Sakamoto, T. Caillat, J.-P. Fleurial, S. Jones, J.-A. Paik, and W. Dong, in *Electroceramic Materials and Applications*, ed. R. W. Schwartz (Wiley, Hoboken, NJ, 2006) Ceramic Transactions, Vol. 196, Chap. 27.
224) J. Tani, M. Takahashi, and H. Kido, IOP Conf. Ser.: Mater. Sci. Eng. **18**, 142013 (2011).
225) G. J. Snyder and E. S. Toberer, Nat. Mater. **7**, 105 (2008).
226) T. Takabatake, K. Suekuni, T. Nakayama, and E. Kaneshita, Rev. Mod. Phys. **86**, 841 (2014).
227) T. Koga, X. Sun, S. Cronin, and M. Dresselhaus, Appl. Phys. Lett. **73**, 2950 (1998).
228) O. Rabina, Y. Lin, and M. Dresselhaus, Appl. Phys. Lett. **79**, 81 (2001).
229) Y. Pei, X. Shi, A. LaLonde, H. Wang, L. Chen, and G. J. Snyder, Nature **473**, 66 (2011).
230) P. Norouzzadeh and D. Vashaee, Sci. Rep. **6**, 22724 (2016).
231) P. Norouzzadeh and D. Vashaee, J. Electron. Mater. **44**, 636 (2015).
232) Y. Tang, Z. M. Gibbs, L. A. Agapito, G. Li, H. S. Kim, M. B. Nardelli, S. Curtarolo, and G. J. Snyder, Nat. Mater. **14**, 1223 (2015).
233) P. Norouzzadeh, C. W. Myles, and D. Vashaee, J. Alloys Compd. **587**, 474 (2014).
234) P. Norouzzadeh, J. S. Krasinski, C. W. Myles, and D. Vashaee, Phys. Chem. Chem. Phys. **17**, 8850 (2015).
235) P. Norouzzadeh, C. W. Myles, and D. Vashaee, Sci. Rep. **4**, 7028 (2014).
236) P. Norouzzadeh, C. W. Myles, and D. Vashaee, J. Appl. Phys. **114**, 163509 (2013).

Amin Nozariasbmarz is currently a Ph.D. candidate in Electrical Engineering (nanoelectronics) with a minor degree in Materials Science and Engineering at North Carolina State University. His B.Sc. and M.Sc. degrees are in Materials Science and Engineering from Sharif University of Technology and University of Tehran, respectively. His main research is on nanostructured and decrystallized thermoelectric materials, particularly on p- and n-type SiGe alloy and its nanocomposites for high temperature power generation applications, and p- and n-type bismuth telluride for body heat harvesting. He has published over 20 papers in peer-reviewed scientific journals.

Aditi Agarwal is currently pursuing M.S. in Electrical Engineering at North Carolina State University. Her research is focused on study of nanostructured bulk materials for thermoelectric and thermomagnetic applications, and calculation of transport properties using Monte Carlo method. Her research interests include solid state physics, nanoelectronics and quantum phenomena. She got her undergraduate degree from Delhi Technological University in New Delhi, India.

Zachary A. Coutant is currently an undergraduate student in electrical engineering at NC State University. His current research is related to the fabrication of thin film thermoelectric devices. His academic interests include solid state physics and devices as well as nano-fabrication.

Michael J. Hall received a B.Sc. in Materials Science and Engineering and a Masters in Nanoengineering at NC State University. Currently working toward a Ph.D. in Materials Science, his research is focused on the fabrication of bulk nanocrystalline and amorphous materials and the study of the electrical and thermal properties of these materials.

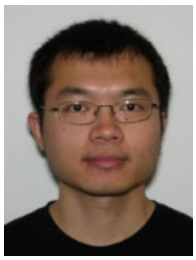

Jie Liu received his Ph.D. degree from Pennsylvania State University in 2013. His Ph.D. work focused on the development of monolithically integrated semiconductor devices by integrating GaN LEDs and Schottky barrier diodes on commercially available LED wafers. He also worked on the investigation of colloidal quantum dot phosphors and LEDs. He obtained his B.S. and M.S. degree in electronics and optical engineering from Tsinghua University, Beijing, China. He joined NCSU as a postdoc in 2015. Currently he is working on development of thin film thermoelectric devices based on SiGe material.

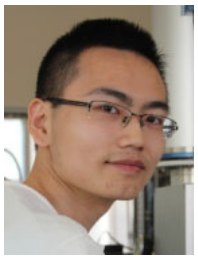

Runze Liu is a Ph.D. student in ECE department, NCSU. Currently he is studying nanostructured n-type bismuth telluride materials.

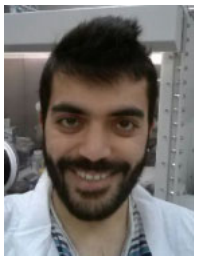

Abhishek Malhotra was born in the town of Jammu in India. He finished his Bachelors of Technology from Manipal Institute of technology, Karnataka in the field of Electronics and Communications. He is presently a Ph.D. student in Electrical Engineering at the North Carolina State University. He is currently working in the field of room temperature bulk thermoelectrics. His research interests include Bulk and Thin film Thermoelectrics, Hydration Sensing and QCMs.

Payam Norouzzadeh received his B.Sc. and M.Sc. degrees in Applied Physics from Sharif University of Technology, and Iran University of Science and Technology, respectively in 1996 and 1999. He received his Ph.D. in Electrical Engineering from Oklahoma State University in 2012 based on his work on application of coherent potential approximation for charge carrier and phonon transport in nanostructured thermoelectrics. He is currently a post-doctoral fellow at Department of Physics and Astronomy, University of Missouri-Columbia working on the application of Density Functional Theory, Molecular Dynamics and Boltzmann Transport Theory for designing novel electronic materials.

Viswanath P. Ramesh completed his Bachelor's degree in Electrical Engineering from Anna University, India in 2013. He is currently working towards a Ph.D. in the Electrical and Computer Engineering specializing in Nanoelectronics and Photonics. His research primarily deals with fabricating flexible Thermoelectric devices for body energy harvesting. His other areas of interest include thin film technology, flexible electronics, MEMS devices, and Aerogel technology.

Yasaman Sargolzaeiaval received her B.Sc. and M.Sc. degrees in Electrical Engineering-Nanoelectronics from Sharif University of Technology in Tehran, Iran, respectively in 2011 and 2013. She worked as a research assistant working on superconductor devices in Superconductor Electronics Research Lab (SERL) in Sharif University for 4 years through her undergraduate and Masters degrees. She is currently a Ph.D. candidate at Department of Electrical and Computer Engineering, North Carolina State University. Her main research activity is fabrication of wearable and flexible thermoelectric generators for body heat harvesting.

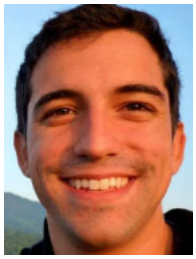

Francisco Suarez completed his Ph.D. in Electrical Engineering from North Carolina State University in 2016. His research was part of the NSF funded Advanced Self-Powered Systems of Integrated Sensors and Technologies (ASSIST) engineering research center, under the direction of Dr. Mehmet C. Oztürk, where he explored the system challenges and design of both rigid and flexible thermoelectric devices for on body wearable power generation. His research interests include renewable energy, energy harvesting, low/self-powered electronics, flexible and stretchable interconnects.

Mehmet C. Ozturk is a graduate of Bogazici University in Istanbul, Turkey in 1980. He received his Ph.D. degree in Electrical Engineering from NC State in 1988. Immediately after graduation, he joined the faculty in his department. He is currently serving as the deputy director of the NSF Sponsored ASSIST Engineering Research Center. Dr. Ozturk's current research interests center around flexible thermoelectric energy harvesting technologies for wearable electronics. He was named an IEEE fellow in 2009 for his contributions in Si and SiGe Epitaxy and their applications in advanced MOS field effect transistors.

Daryoosh Vashaee is an expert in superlattices and nanostructured materials for energy conversion and sensing applications. In the past, he has contributed to the development of several key thermoelectric structures including heterostructure thermionic devices and bulk nanocomposite thermoelectric materials. He is the recipient of the NSF CAREER award and the Goldsmid Award for research excellence in thermoelectrics from the International Thermoelectric Society. He received his Ph.D. from University of California at Santa Cruz in 2004, worked at MIT as postdoctoral scholar, at Oklahoma State University as assistant professor, and joined North Carolina State University ECE department as associate professor in 2014.